Dielectric features of Au_2O_3 doped Li_2O-SiO_2 glass system-Influence of Pb_3O_4

T.V.N. Keerti Kut[a,b], A. Bafti[c], J. Pisk[d], L. Pavić[e*], A. Venkata Sekhar[a], P. Naresh[f], A. Siva Sesha Reddy[g], G. Naga Raju[a], V. Ravi Kumar[a], N. Veeraiah[a, h*]

[a]Department of Physics, Acharya Nagarjuna University, Nagarjuna Nagar- 522 510, India,
[b]Department of Physics, Rajiv Gandhi University of Knowledge Technologies, IIIT Nuzvid, India
[c]Faculty of Chemical Engineering and Technology, University of Zagreb, 10000 Zagreb, Croatia
[d]Department of Chemistry, Faculty of Science, University of Zagreb, 10000 Zagreb, Croatia
[e]Ruđer Bošković Institute, Division of Materials Chemistry, 10000 Zagreb, Croatia
[f]Department of Physics, Potti Sriramulu Chadalavada Mallikarjuna Rao College of Engineering & Technology, Vijayawada, Andhra Pradesh 520 001, India
[g]Department of Physics, Krishna University, Machilipatnam-521004, Andhra Pradesh, India.,
[h]Department of Physics, Andhra Loyola College (Autonomous), Vijayawada, A.P., India

Abstract

Studies on dielectric properties viz., ε' (dielectric permittivity), M, Z and σ_{ac} as functions of frequency and temperature (over wide ranges), of glasses/glass-ceramics give quantitative information on their insulating character. Such studies are also useful for understanding structural aspects of these glasses to a great extent. In this work Pb_3O_4 mixed Li_2O-SiO_2:Au_2O_3 glasses were synthesized and heat-treated. Analysis of the results of various characterization techniques indicated increased degree of internal augmentation of the samples. Observed decrease of ε' with Au_2O_3 up to 0.04 mol% was attributed to the decreased magnitude of space charge polarization due to growing presence of PbO_4 units. Dipolar relaxation effects of these samples were evaluated using Cole-Cole plots. Variation of conductivity with Au_2O_3 concentration was analyzed using polaronic tunneling model. Conclusions of these results were found to be in in concurrence with spectroscopic studies. Overall, the presence of Pb_3O_4 caused reduction the conductivity of these glasses.

***Keywords*:** Pb_3O_4; Au ions; Li_2O-SiO_2 glasses; Dielectric studies; A.C. conductivity

*Corresponding authors: lpavic@irb.hr; nvr8@rediffmail.com

1. Introduction

Investigation of dielectric properties of glass or glass-ceramic materials gives information on their insulating character as well as their structural aspects to a great extent. Such information can be obtained by measuring a variety of dielectric parameters viz., ε' (dielectric permittivity), M, Z and σ_{ac} as functions of ω and T (over large ranges) and also in terms of their chemical composition. A vast number of similar investigations were reported on a variety of glass systems in the recent past by different researchers [1–6].

Among different alkali silicate glass systems, Li_2O was predicted to form stable glasses with SiO_2at about 1400 ºC. Nevertheless, such glasses were found to devitrify easily the another alkali SiO_2 glass systems [7]. Strictly speaking, stable Li_2O-SiO_2 glasses can be obtained with SiO_2concentration of more than 70 %. To reduce the devitrification, lead oxide was mixed to Li_2O-SiO_2 glass system in the present investigation. Lead oxide takes part in the glass system as a network former and also acts as a modifier. Among different oxides of Pb, Pb_3O_4 (red lead) was considered as a fascinating heavy metal oxide since it causes to increase the density and also refractive index of the host glass to a larger extent and increases the practical utility of the glasses. Some of the applications of lead oxide mixed glasses include non-linear optical devices, electrolytes in solid-state batteries etc. Pb_3O_4 in fact decomposes in to PbO at about 600 ºC as per the chemical equilibrium $2Pb_3O_4 \rightarrow 6\ PbO + O_2\uparrow$. In this process, two polymorphs namely, α-PbO_2 and β-PbO_2 do form in the midway before PbO is evolved. Among these two intermediate phases, α-PbO_2 is more unstable, whereas β-PbO_2 is relatively stable and possesses low electrical resistivity and reported to high corrosion resistant even in low pH media [8, 9]. Among various practical utilities of red lead, its application as cathode in lead-acid batteries is remarkable [10, 11]. Nevertheless, during the melting even β-PbO_2 gets converted into PbO by capturing $2e^-$. The

Pb ions in PbO_2 do form PbO_4 groups and make cross-links with silicate groups, while Pb^{2+} ions in PbO were predicted to act as modifiers predominantly [12–14].

According to different crystallographic investigations, the Pb-O coordination geometries are of 2 kinds viz., holodirected and hemidirected. In holodirected, the Pb ligand bonds are dispersed on the entire surface of a surrounding sphere and exist approximately in tetrahedral structures. As per Cambridge Structural Database, all Pb(IV) groups have a holodirected configuration [15], whereas Pb(II) groups are hemidirected for lower coordination (2-5); in these, Pb–bonds pointed throughout only a portion of an encircling sphere, viz., a distinguishable cavity in the spreading of bonds to the ligands like pyramidic groups do exist as shown in Fig. 1.

Pb(II) with [Xe] $4f^{14}5d^{10}\,6s^2$ electron configuration exhibits ‘‘inert-pair effect” [15, 16]. It indicates that this pair of electrons resist either exclusion or contribution to the formation of covalent bond with the outer electrons on Pb(II). It is because the 6*s* orbital contracts and increases the required energy either for removal or to interact with $6s^2$ electrons. Whereas *d* and *f* orbitals are weakened since they enlarge radially outwards because of shielding of *s* and *p* electrons from the attraction of nucleus. In consequence, a stable and comparatively inert outer lone pair of electrons associated with divalent lead ions does exist [15, 16]. Overall, because of the existence of lead ions in diverse valence states in Pb_3O_4, it is quite likely that this oxide influences the transport of Li^+ ions to facilitate increase of σ_{ac} in the lithium silicate glass network.

Additionally, by admixing traces of noble metallic ions like Auto Li_2O-Pb_3O_4-SiO_2 (LPS) glass system, interesting and useful variations in the dielectric properties of these glasses are expected. In general, the glasses containing noble metal ions (like Au, silver) show surface plasmon resonance (SPR) due to interaction of the incident e. m. wave. This resonance

stimulates a strong local electric field in the vicinity of these ions [17] and affects the dielectric characteristic of the host glass to a greater extent. Quite recently we have reported the detailed studies on the impact of Ag ions on dielectric characteristics of Li_2O-Pb_3O_4-SiO_2 glass ceramics [18]. These studies indicated that red lead acted as an obstacle for the enhancement of the conductivity in such fast ion conducting glasses.

Motivated by these facts, a small amount of gold oxide (Au_2O_3) was added to LPS glass system and its dielectric properties were investigated in this study. Au_2O_3 decomposes easily into AuO, Au_2O and Au^0metallic particles (MPs) during the glass formation. Among these, the gold MPs do act as modifiers and de-fragment the glass network [19]. Such de-augmented network facilitates a decrease of electrical impedance Z or increase of σ_{ac}. Overall, the presence of Au^0 MPs was predicted to be an advantage for achieving interesting alterations in the dielectric features of the chosen glass system. To ensure the entrenchment of gold MPs in the host glass, the glass samples were heat-treated for 4hat the temperature of crystallization (T_c). During heating there is a possibility for Au^{3+} ions to be reduced to Au^0 MPs as per the reaction: $Au^{3+} \rightarrow Au^{2+} \rightarrow Au^{+} \rightarrow Au^0$. For these reasons, the conduction in these samples is predicted (i) due to exchange of polarons between Au ions of polyvalence states and also in between and divalent and tetravalent lead ions and (ii) furthermore because of the diffusion of Li^+ ions.

This study consists of (i) details of the methods of preparation of LPS glasses added with small amounts (0 to 0.08 mol%)of Au_2O, (ii) methods of characterization of the samples by XRD, SEM, XPS and DSC techniques, (iii) the structural analysis of these samples in terms of Au_2O_3 concentration by different spectroscopic methods (viz., IR, OA and XPS) and (iv) quantitative studies on various dielectric quantities that include ε, M, dipolar relaxation phenomenon, impedance spectra and σ_{ac} over a broad region of frequency viz., 10^{-2} to 10^6 Hz

and in the temperature region 30 to 250ºC and (iv) the analysis of obtained results as a function of Au_2O_3 concentration.

2. Experimental

$(40\text{-}x)Li_2O–10Pb_3O_4–50SiO_2:xAu_2O_3$ (where x = 0, 0.01, 0.02, 0.04, 0.06, and 0.08), all in mol %, was the composition selected for this study and the samples were, respectively, labelled as Au_0, Au_1, Au_2, Au_4, Au_6 and Au_8. Glasses were prepared by the melt-quenching technique. Mixtures of proportionate amounts of analar grade reagent compounds were transferred in to pt crucibles and liquefied at 1400 °C for1/2 h. Obtained melt was discharged into brass moulds and to ensure the samples free from internal bubbles, cracks, etc., they were annealed at about 350 °C. The obtained samples were heated at 250 °C for 4 h and were quenched to ambient temperature to get the entrenchment of gold metallic particles (Au^0 MPs) in the samples. Later they were finely polished to the final dimensions of about 1.0 cm^2surface area and 0.2 cm thickness.

A Carl Zeiss –EvoMA15A scanning electron microscope was used to record SEM pictures of the glasses. The energy dispersive spectra (EDS) of the samples were recorded to verify their chemical make-up using Oxford-INCA Penta FETX3. XRD studies were performed on a RIGAKU-D/MaxULTIMA III X-ray diffractometer in the 2θ range of 15– 65 degrees in the intervals of 0.02 deg/s. Mettler TGA/DSC 3+ thermos-balance was used to study the thermal behaviour of these samples. Analysis were performed in Pt crucible on powder samples (~40 mg) in the temperature range 25 - 1000 °C heated @ 20 °C per min. in O_2 atmosphere. Mettler STARe 9.01 software was used to analyse the results.

PHI 5000 Versa Probe ULVAC instrument with a monochromatic Al Kα (1486.6 eV) source was used to record XPS. These spectra were recorded with respect to C 1*s* peak (284.6

eV). FT-IR spectra were registered to a precession of 0.1 cm^{-1} on a pre-calibrated Shimadzu IR TRACER 100 spectrophotometer in ATR mode. Optical absorption (OA) spectra were recorded on A JASCO UV-VIS-NIR spectrophotometer in the spectral range of 200–2000 nm. For dielectric measurements thin gold electrodes (of about 6 mm diameter), were sputtered on either surface of the samples. Dielectric measurements and σ_{ac} were performed on Novocontrol Alpha-AN Dielectric Spectrometer in the frequency region 0.01 – 1.0 MHz and in the temperature range of 30 - 250 ºC (±0.2ºC). Complex impedance diagrams were analysed using equivalent circuits modelling.

3 Results and discussion

As-prepared LPS glass samples with no Au_2O_3 were observed to be colourless. With the introduction of Au_2O_3 from 0.01 to 0.04 mol%, the colour of the samples was gradually changed from slight ruby to pale yellow (Fig. 2). Such observation suggested the presence of maximum concentration Au^0 MPs in the glasses consisting of low quantity of Au_2O_3 [19, 20]. With the measured value of density of the samples, the concentration of Au^{3+}ions and average Au^{3+} ion separation were calculated and presented in Table 1.

Powder X-ray diffractograms of as-prepared glasses did not exhibit any sharp peaks and indicated virtual absence of crystallinity in these samples. Nevertheless, the diffractograms (Fig. 3) of the post-heated glasses exhibited diffraction peaks at 28.7º and 44.0º, identified as being due to the reflections from Au_2O_3 (400) and Au^0 (200) metallic particles [21]. With the increase of Au_2O_3 up to 0.04 mol%, the intensity of the peak connected with gold metallic particles exhibited a decrease. Such a decrease indicated a minimal concentration of Au^0 metallic particles in the sample Au_4.

SEM images of heat-treated LPS glasses containing various contents of Au_2O_3 were shown in Fig. 4. The images indicated that randomly distributed crystal grains (with a few μm in size) were entrenched in the residual amorphous phase. With increase of Au_2O_3 content up to 0.04 mol%, the volume fraction of crystallites seemed to be decreased. The chemical make-up of the samples verified by EDS (Fig. 4) suggested the intact of all the anticipated elements in the glass matrix.

XPS spectra of the glasses were recorded to understand the variation of the concentration of Au^0 MPs with the concentration of Au_2O_3 in these samples. In Fig. 5 (a), the deconvoluted and fitted spectra of Au^0 and Au^{3+} ions in the glasses Au_1 and Au_4 were shown. The spectra exhibited peaks at 85.8 eV and 89.6 eV (corresponding to binding energy of 4f Au^{3+} ions) and two other peaks at 84.0 eV ($4f_{7/2}$) and 87.6 eV ($4f_{5/2}$) related to Au^0 MPs [22]. In the inset of this figure. The intensities of the peaks located at 84.0 eV (BE of Au^0 MPs) and 85.8 eV (BE of Au^{3+} ions) were plotted against the concentration of Au_2O_3. The plots indicated a gradual decay of the peak related to Au^0 MPs with an increase of Au_2O_3 up to 0.04 mol% with simultaneous increase of the peak related to Au^{3+} ions.

In Fig. 5 (b), XPS spectra of glass (Au_2) registered in $4f_{7/2}$ and $4f_{5/2}$ region of Pb were presented. The deconvoluted $4f_{7/2}$ spectrum exhibited three peaks at 137.5, 137.9 and 138.4 eV connected with PbO_2, PbO and Pb_3O_4. The spectrum also exhibited three other peaks at 142.36, 142.76 and 143.26 eV (Pb $4f_{5/2}$ region) ascribed to PbO_2, PbO and Pb_3O_4 [18]. In the inset of Fig. 5 (b), the intensities of PbO_2 ($4f_{7/2}$) peak and Pb_3O_4 peak ($4f_{7/2}$) were plotted with the concentration of Au_2O_3. The plots indicated that as the concentration of Au_2O_3 was increased up to 0.04 mol %, the intensity of PbO_2 peak showed a study increase with simultaneous decrease of Pb_3O_4 peak. Such result revealed an increased presence of Pb(IV)-O bonds in the network of this

glass that paved the way for the increased degree of internal polymerization. XPS studies thus revealed that internal degree of augmentation was maximal in the sample Au_4 and such polymerized glass network is expected to offer the maximal resistance for the diffusion of conducting species that would contribute to σ_{ac}.

In Fig. 6, DTA traces of these samples were presented. The traces indicated a weak endothermic change due to glass transition in the temperature region 375–400 ^{o}C. A strong exothermic peak followed by multiple weak peaks (attributed to the entrenchment of one or more crystal grains) were observed in the temperature region 510–540 ^{o}C. A brief summary of these results was presented in Table 2. The results suggested the largest value of T_{c1}-T_g for Au_4 glass and indicated a low magnitude of de-vitrification of this glass when compared with other glasses.

In Fig. 7 (a), the OA spectra of Au_2O_3 doped lithium lead silicate glasses recorded in the spectral range 250–800 nm were shown. The spectrum of Au_2O_3 free glass indicated cut-off wavelength at 330.5 nm. With the addition of Au_2O_3 from 0.01 to 0.04 mol%, the edge exhibited spectrally blue shift and shifted towards longer wavelength for further increase of Au_2O_3 content. The optical bandgap E_o of the glasses was evaluated by drawing Tauc plots (Fig. 7 (b)). E_o was observed to be the maximal for the glass Au_4 (inset of Fig. 7(b)). From the XPS studies, it was noticed that there was an increase in the concentration of Pb^{4+} ion as Au_2O_3 content was increased up to 0.04 mol%. Such Pb^{4+} ions do occupy network forming positions and form Pb^{IV}-O-Si^{IV} linkages. Such type of polymerisation caused a reduction of the degree of localization of free electrons, lowered the concentration of donor centres and caused to enlarge the optical bandgap as observed.

Moreover, the interactions of *p*- electrons of lead and *d*- electrons of Au ions also caused the enlargement of the optical bandgap. XPS and also XRD results suggested that there was a

decreased proportion of Au^0 metallic particles with an increase of Au_2O_3 content up to 0.04 mol% or there was a lowering of the concentration of donor centres. As a result, the trapped electrons at energy states of Au^{3+} ions were separated to a longer distance with the unfilled 4*d* energy states of Au^0 particles. For this reason, the width of the energy band containing the energy states of Au^0 impurity, shrunk in the bandgap of the glass and caused increase of E_o with Au_2O_3 content up to 0.04 mol%.

Additionally, an absorption band was visualized in these spectra in the wavelength region 460–600 nm. Normally, the Au^0 metallic particles do form the clusters in the material and such clusters exhibit SPR with coherent oscillations of electrons and the incident e.m. waves upon the surface of the clusters[23].

The observed absorption band in these spectra was due to such resonance. Furthermore, this band showed a decaying trend with Au_2O_3 content up to 0.04 mol%. This observation suggested decreasing fraction of Au^0 particles with an increase of Au_2O_3 concentration in the samples. Moreover, the SPR band indicated a blue shift up to 0.04 mol% of Au_2O_3. Such blue shift suggested the decreasing dimensions of the clusters of gold nanoparticles that changed the absorption from multi-poles to dipoles etc. [24-26].With the help of the relation $R_G = V_F\lambda^2/2\pi c\Delta\lambda$ [21] (V_F represents the Fermi velocity), the approximate size of the Au^0 nanoparticles (R_G) was evaluated and it was found to be the minimal in the glass Au_4. Overall, the OA spectral results suggested that there was a decreasing fraction of gold metallic particles with decreasing size in the studied glasses with Au_2O_3 content from 0.01 to 0.04 mol%.

The FT-IR spectra of these samples (Fig. 8) exhibited two principal peaks due to asymmetric and symmetric stretching vibrations O–Si–O of SiO_4 groups approximately at 1010 and 795 cm^{-1}, respectively [27]. Spectra further indicated two other peaks at 575 cm^{-1}

(recognised as being due to the Pb(IV)-O vibrations bond of PbO_4 groups [8]) and at 462 cm^{-1} (a band due to Pb(II)-O stretching [27]). As the concentration of $Au_2O_3$was increased up to 0.04 mol%, the symmetrical stretching band of O–Si–O bonds and also that of PbO_4 units exhibited a growing tendency. Such growth of these bands suggested a possible increased degree of structural augmentation. Beyond 0.04 mol% of Au_2O_3 concentration, a reversal trend of these bands was observed. In Table 4, a summary of the positions of various bands observed in IR spectra was presented.

Variation of dielectric constant $\varepsilon'(\omega)$ with frequency measured for the glass Au_1 was presented in Fig. 9 (a), whereas in Fig. 9 (b) its variation with temperature for the glass Au_2 was presented. $\varepsilon'(\omega)$ was observed to decrease with increase of frequency and reached a high-frequency plateau value $\varepsilon'_\infty(\omega)$. At larger T, $\varepsilon'(\omega)$ showed a larger dispersion with larger values at low frequency. It was the space charge polarization (which represents building up of conducting species near electrodes) that caused to enhance the value of $\varepsilon'(\omega)$ at low frequency Normally, its magnitude depends on the long range diffusion of conducting species. To be clearer, the observed larger increase of $\varepsilon'(\omega)$ especially in the low frequency range was because of the easy migration of charge carriers in the glass sample. In the high frequency region, the frequency of oscillation of these species was comparatively lower and hence, $\varepsilon'(\omega)$ reached a high-frequency plateau $\varepsilon'_\infty(\omega)$ (Fig. 9(a)).

In Fig. 9(a) inset, the variation of $\varepsilon'(\omega)$ with the content of $Au_2O_3$was presented at a frequency of 1 kHz and 250 ^oC. $\varepsilon'(\omega)$ exhibited a decrease with Au_2O_3 concentration upto 0.04 mol% and beyond that, it exhibited an increasing tendency. The results of XPS, as well as IR spectral studies, indicated the maximal presence of Pb^{4+} ions that occupied tetrahedral positions and cross-linked with SiO_4 units in this glass network. Such linkages hindered the movement of

conducting species towards electrodes [28, 29] and caused to decrease in the value of the dielectric constant with an increase of Au_2O_3 up to 0.04 mol%.

The plots of $\varepsilon''(\omega)$ *vs* frequency and temperature for Au_8 glass were shown in Figs. 10 (a and b), respectively. Variations suggested no dipolar relaxation effects in the studied frequency region; probably electrode effects were dominating in this frequency range. In order to ascertain dipolar effects more clearly electric moduli notation was followed. As per this notation, M^* (complex electric modulus), is represented by

$$M^* = M' + iM'', \qquad (1)$$

$$\text{where, } M' = \frac{\varepsilon'(\omega)}{(\varepsilon'(\omega))^2 + (\varepsilon''(\omega))^2} \qquad (2)$$

$$\text{and } M'' = \frac{\varepsilon''(\omega)}{(\varepsilon'(\omega))^2 + (\varepsilon''(\omega))^2}. \qquad (3)$$

The values of M' and M'' were estimated using ε' and ε'' and the variations of these two parameters with frequency at different temperatures and with temperature at different frequencies were shown in Figs. 11 (a) and 11(b), respectively, for the glasses Au_2 and Au_8. These figures exhibited a distinct dipolar relaxation phenomenon.

From the points of intersection of these two moduli at resonance frequency ω_r, the dipolar relaxation time τ was evaluated and the dependence of τ on temperature in the high-temperature range was shown in Fig. 12 for the studied glasses. The variation indicated decreasing trend of τ with temperature and appeared to be near temperature independent. The value of τ (evaluated at a given temperature T) with Au_2O_3 concentration was observed to be the largest for the glass Au_4 (Table 5). Using the equation, $\tau = \tau_o \exp(W_d/k_BT)$, W_d, the activation energy for dipoles was determined from $\ln\tau$ *vs* $1/T$ plots and presented in Table 5. W_d was found to be the maximal for

the glass Au_4. This observation suggested minimal freedom for dipoles to orient in the field direction in this glass.

For further analysis of the dipolar phenomenon of these glasses, Cole-Cole plots were drawn between M'' *vs* M' at high temperatures and shown in Fig. 13. These diagrams seemed to be semi-circular arcs with centers depressed below the abscissa. The estimated value of spreading factor viz., the angle (α') between a line passing through the center of the arc and the *X*-axis (at the origin), was shown in Table 5. α' exhibited a decreasing trend with Au_2O_3 content (up to 0.04 mol%) and indicated decreased magnitude of distribution of τ. Normally, the presence of multiple kinds of dipoles with varied dipole moments was reported to be accountable for the spreading of relaxation time [30]. Additionally, the dipoles that were entrenched in asymmetrical potential in the glass matrix also contributed to such dispersion [7]. The lowering of α' indicated a lowered degree of asymmetric environment for the dipoles as was also evidenced by IR spectra. The Pb^{2+} ion complexes with oxygens do possess dipole moment and contributed to dipolar effects. The larger presence of tetravalent Pb ions (in the glass sample Au_4) that occupied network forming positions resisted the liberty for dipoles to the 'to and fro' movement and caused to increase dipolar activation energy W_d as was observed.

In Figs. 14 (a) and 14 (b), the plots of Z' and Z'' (real and imaginary components of impedance) *vs* ω were drawn for the glass Au_4. Among these two components, the Z' (a pure resistance part) exhibited a decreased trend with ω (with a meagre non-linearity in the lowerω region due to the electrode effect), whereas the other component Z″, indicated large dispersion with *T* in the lowerω ranges (< 1 kHz). Further, up to about 1 kHz, Z″ indicated a linear increase with ω particularly at larger *T* and indicated the behaviour of the inductive

reactance ($L\omega$). Beyond 1 kHz, Z'' exhibited an inverse proportionality with ω (typical capacitive reactance, *viz*., $1/C\omega$).

To understand the dependence of the magnitude of the impedance of the studied glasses on the concentration of Au_2O_3, the plots between Z'' *vs* Z', known as impedance plots (or Nyquist plots), were drawn in different intervals of temperatures and were shown in the Figs. 15 (a-d) for the glass Au_1. The area under the curve showed a decay with temperature and it is suggestive of decrease of impedance of the glasses with temperature. The graphs appeared to be semi-circular shapes followed by an inclined spur (at lower frequency and higher temperature ranges) due to thermally activated diffusion of the charge carriers in the high temperature range.

The comparison plots of impedance for Li_2O-Pb_3O_4-SiO_2:Au_2O_3 glasses were drawn at 250 °C (Fig. 15 (e)). As Au_2O_3 content was raised to 0.04 mol%, the area under the curves was found to increase and suggested the maximal magnitude of impedance for the glass Au_4. The magnitude of the inclined spur was found to be minimal for this glass and suggested that the thermally stimulated mobility of the charge carriers was the lowest for this glass.

To throw more light on impedance behaviour, Bode plots ($|Z|$ and φ = arc tan (Z''/Z') *vs* ω) were drawn and presented in Fig. 15 (f) for a selected glass Au_2 at 200 °C. The plot indicated decrease of $|Z|$ with the increase of frequency and such behaviour suggested that electronic (or Faradic) current contribution to Z [31].

In the Figs. 16 (a) and 16 (b), the plots of $\ln\sigma_{ac}$ versus ω and also *vs* $1/T$ for Au_6 glass were plotted, respectively. These figures suggested that in the larger temperature and in the lower frequency range, the variations are near frequency independent (viz., $\sigma_{ac}(\omega) \rightarrow \sigma_{dc}$). Moreover, the plots were seemed to be nearly independent of temperature in the larger ω and lower T ranges. However, in the intermediate frequency range, it was found to be varied linearly with ω viz., σ_{ac}

$(\omega) \propto \omega$. Overall, it appeared that the relation $\sigma_{ac}(\omega) \propto \omega^{s}$ was valid ($s = 1$ in the larger frequency and lower temperature ranges) and it represents the universal dielectric response (UDR) exponent. In general s<1.

In the middle frequency range, a backward and forward hopping of charge carriers occurred due to Columbic repulsion. The results of structural investigations described earlier, indicated that lead and Au ions existed in different valence states in these glass samples. Hence, the polarons exchanged between Pb^{2+} and Pb^{4+} and Au^{0} to Au^{3+} ions contributed to σ_{ac}. This contribution was further more to the transport of lithium ions. Variation of σ_{ac} (at 1 kHz and 250 °C) with Au_2O_3 content was shown in the inset of Fig. 16 (a). The figure exhibited minima at 0.04 mol% Au_2O_3. Using the ln σ_{ac} *vs 1/T* plots, the activation energy W_{ac} was estimated and it was observed to be the maximal for the glass Au_4 (Table 5). Such high value suggested the minimal free space accessible for the migration of charge carriers in this glass.

From the slopes of log $\sigma_{ac}(\omega)$ *vs* log ω plots (in the middle frequency range), the UDR exponent *s* was estimated at various temperatures. Such plots for Au_6 glass were shown in Fig. 17. The exponent *s* was observed to decrease with temperature (inset of Fig. 17). The decrement of *s* with temperature indicated that conduction was due to polaronic tunneling [32]. However, variation of *s* with Au_2O_3 content (at a given temperature) indicated a maximum for the glass Au_4 (Table 5). Such a larger value indicated that the accessible free volume for the transport of Li^{+} ions was the lowest in this sample [33]. The results of the structural analysis suggested that samples containing 0.04 mol% of Au_2O_3, possessed the maximal Pb^{IV}-O groups that were predicted to augment with SiO_4 groups. Such links hindered the diffusion of Li^{+} ions and in consequence, a decrease in the conductivity was observed.

It was already mentioned that σ_{ac} with T in the low T range (particularly in the larger - ω region) was near invariant. In this region, the behaviour of σ_{ac} was evaluated using the quantum mechanical tunneling (QMT) model [34]. Based on this mechanism, the density of defect energy states $N(E_F)$ near the Fermi level, was evaluated using the expression:

$$\sigma(\omega) = \frac{\pi}{3} e^2 k_B T \left[N(E_F)\right]^2 \alpha''^{-5} \omega \left[\ln \frac{\nu_{ph}}{\omega}\right]^4, \quad (4)$$

In Eq. (4), $\left[\ln\left(\frac{\nu_{ph}}{\omega}\right)\right]$ represents hopping distance of the conducting species. The details of the other parameters of Eq. (4) were reported in Ref [31]. The values of $N(E_F)$ were evaluated, using Eq. (4) at 105 kHz and 355 K, with average value of α'' as 0.65 $(Å)^{-1}$(evaluated from the plots of $\log \sigma_{ac}$ *vs* R_i), and presented in Table 5. $N(E_F)$ was found to be the minimum for the glass Au_4, which indicated the lower fraction of structural defects in this glass. Such a result was found to be in agreement with the results of spectroscopic studies.

4 Conclusions

The results of characterization and dielectric properties of red lead mixed Li_2O-SiO_2 glasses doped with different concentrations of Au_2O_3 were reported.

The salient features of the results of these studies and conclusions drawn are as follows.

1. The results of characterization techniques (viz., XRD, XPS, optical absorption, IR studies) of these glasses suggested that the glasses were composed of Au^{3+}, Au^0 metallic particles, along with lead ions in Pb^{4+}, Pb^{2+} valence states.

2. As the concentration of Au_2O_3 was increased from 0.01 to 0.04 mol%, the colour of the samples was gradually changed from slight ruby to pale yellow. From this observation it was concluded that the presence of maximum concentration Au^0 metallic particles in the glasses consisting of low quantity of Au_2O_3

3. The XRD studies indicated that the intensity of the peak related to Au^0 metallic particles exhibited a decreasing trend with increase of Au_2O_3 up to 0.04 mol%. This observation suggested a minimal concentration of Au^0 metallic particles in the glass Au_4.
4. XPS studies revealed that there is a gradual decrease in the concentration of Au^0 metallic particles with simultaneous increase in the concentration of Au^{3+} ions with increase of Au_2O_3 concentration up to 0.04 mol%. These studies have also indicated an increased presence of Pb(IV)-O bonds (that are expected to pave the way for the increased degree of internal polymerization) in the glass network. As a whole, the XPS studies suggested maximal internal degree of augmentation in the sample Au_4 and such polymerized glass network was predicted stiffly resist the diffusion of conducting species that would contribute to σ_{ac}.

5. The dielectric constant ε' exhibited a decreasing trend with increase of Au_2O_3 content up to 0.04 mol%. Such decrease was ascribed to the lowering magnitude of space charge polarization due to the decreased fraction of free space defects (because of the presence of low concentration of Au^0 metallic particles that act as modifiers) in the glass matrix.

6. The dipolar effects exhibited by electric moduli of these glasses were evaluated using Cole-Cole diagrams. The divalent lead ion complexes with oxygens were predicted to contributed to dipolar effects. The observed maximal value of dipolar activation energy W_d for the glass Au_4 was ascribed to the presence of larger concentration of tetravalent Pb ions that occupied network forming positions and resisted the dipoles to orient in the field direction.

7. The mechanism of a.c. conductivity was analyzed using polaron exchange between lead ions and also between Au ions of different valence states. The diffusion of Li^+ was also found to contribute to the conductivity. The observed minimal of conductivity in the glass containing 0.04 mol% of Au_2O_3 was attributed to the maximal degree of augmentation between various various structural units in this sample

The presence of red lead in the glass material is in general is advantageous in improving the density as well as refractive index and make the glasses useful for NLO device applications. However, in the Li_2O-SiO_2 glass doped with different concentrations of Au_2O_3, its presence caused an obstruction for the progressive diffusion of Li^+ ions and caused to decrease the conductivity with increase of Au_2O_3 up to 0.04 mol%.

Acknowledgement

J.P. acknowledge the support of project CIuK co-financed by the Croatian Government and the European Union through the European Regional Development Fund-Competitiveness and Cohesion Operational Programme (Grant KK.01.1.1.02.0016.).

References

[1] C. Devaraja, G. V. Jagadeesha Gowda, B. Eraiah, Asha M. Talwar, A. Dahshan, S.N. Nazrin, Structural, conductivity and dielectric properties of europium trioxide doped lead boro-tellurite glasses, J. Alloys Compd. 898 (2022) 162967.

[2] Mohammed A. Algradee, Y.H. Elbashar, A.B. Alwany, H.H. Hassan, R. El-Mallawany, Impact of Yb_2O_3 on the physical, bonding, dispersion and dielectric properties of Li_2O–ZnO–P_2O_5 glasses, Mater. Sci. Semicond. Process. 140 (2022) 106362.

[3] Crystallization and dielectric properties of oxyfluoride alumina silicate glasses added with Na_2O, X. Shao, Y. Hu, Y. Zhao, S. Chen, L. Liu, J. Chen, J. Li, J. Non-Cryst. Solids 576 (2022) 121261.

[4] J. Li, J. Huang, H. Feng, X. Wang, X. Yin Y. Zhang, Effect of TiO_2/SiO_2 molar ratio on the structure, dielectric and crystallization properties of SiO_2-TiO_2-ZrO_2-RO-Al_2O_3 glasses, J. Non-Cryst. Solids 576 (2022) 121243.

[5] Q. Chen, Z. Li, H. Wang, Influence of polarization, multi-valences and multi-coordination of cobalt: Third-order nonlinear, dielectric and Faraday properties of Bi0.5Co1.5S3/high optical basicity glass, Mater. Res. Bull. 145 (2022) 111531.

[6] G. El-Damrawi, A.M. Abdelghany, M.A. Madshal, AC conductivity and dielectric properties of Cr_2O_3 doped SrO–P_2O_5 glasses, Physica B 618 (2021) 413184.

[7] S. R. Elliott. Physics of amorphous materials, Longman, Essex, 1990.

[8] D. Guo, C. Robinson, J.E. Herrera, Mechanism of dissolution of minium (Pb_3O_4) in water under depleting chlorine conditions, Corrosion Science 103 (2016) 42–49

[9] H. Zhang, S.H. Liu, F. Liu, S.L. Yan, W.Y. Li, Study on the reaction mechanism between Pb_3O_4 and Si in stored silicon delay composition, J. Thermal Analysis Calorim. 132 (2018):327–336.

[10] Greenwood N. Norman, Earnshaw Alan Chemistry of the Elements (2nd ed.). Butterworth-Heinemann. Amsterdam, 1997.

[11] François Cardarelli Materials Handbook: A Concise Desktop Reference. Springer. New York, 2008.

[12] A. Siva Sesha Reddy, G. Lakshminarayana, N. Purnachand, V.R. Kumar, N. Venkatramaiah, V. Ravi Kumar, N. Veeraiah, Influence of gold ions on visible and NIR luminescence features of Er^{3+} ions in lead boroselenate glass ceramics, J. Lumin. 226 (2020) 117481.

[13] A. Subba Rao, I.V. Kityk, J. Ashok, V. Ravi Kumar K.J. Plucinski, A. Siva Sesha Reddy, K. Naresh Kumar, N. Veeraiah, Physical characteristics of $PbO-ZrO_2-SiO_2:TiO_2$ glass ceramics embedded with $Pb_2Ti_2O_6$ cubic pyrochlore crystal phase: Part-II piezo-optical acoustic and elastic Properties, J. Alloys Compd. 725 (2017) 318-325.

[14] Ch. Chandrakala, A. Siva Sesha Reddy, M. Kostrzewa, N. Purnachand, N. Venkatramaiah, G. N. Raju, V. Ravi Kumar, N. Veeraiah, Dielectric relaxation dynamics and polaronic tunneling conduction mechanism of electrical conductivity of Fe_2O_3 doped $PbO–ZrO_2–SiO_2$ glass ceramics, Phys. Status Solidi (a) 1 (2021) 2100071.

[15] Liat Shimoni-Livny, Jenny P. Glusker, Charles W. Bock, Lone Pair Functionality in divalent lead compounds, Inorg. Chem. 37 (1998)1853-1867.

[16] Martin Breza, Lukáš Bucˇinsky´, Stanislava Šoralová, Stanislav Biskupic, On the origin of the hemidirected geometry of tetracoordinated lead (II) compounds, Chem. Phys. 368 (2010) 14–19.

[17] B. Sahu, R. Dey, P.K. Bajpai, Au^{3+} ion implantation on FTO coated glasses: effect on structural, electrical, optical and phonon properties, Nucl. Instrum. Methods Phys. Res. B. 400 (2017) 11–21.

[18] T.V.N. Keerti Kut, Sara Marijan, Jana Pisk,A. Venkata Sekhar, A. Siva Sesha Reddy, N. Venkatramaiah,G. Naga Raju,L. Pavić, N. Veeraiah, Impact of silver ions on dielectric properties and conductivity of lithium silicate glass system mixed with red lead, J. Non-Cryst. Solids 588 (2022) 121641.

[19] A. Siva Sesha Reddy, M. Kostrzewa, P. Pavani Koteswari Devi, N. Purnachand, A. Ingram, N. Venkatramaiah, V. Ravi Kumar,N. Veeraiah,Dielectric dispersion impedance spectroscopy and polaron tunneling phenomenon in Au_2O_3 mixed $PbO-B_2O_3-SeO_2:Er_2O_3$ glass ceramics, J. Alloys Compd. 904 (2022) 164069.

[20] R.H. Lambertson, C.A. Lacy, S.D. Gillespie, M.C. Leopold, R.H. Coppage, Gold nanoparticle colorants as traditional ceramic glaze alternatives, J. Am. Ceram. Soc. 100 (2017) 3943–3951.

[21] J. Ashok, M. Kostrzewa, M. Srinivasa Reddy, V. Ravi Kumar, N. Venkatramiah, M. Piasecki, N. Veeraiah, Structural and physical characteristics of Au_2O_3 doped sodium antimonate glasses-part I, J. Am. Ceram. Soc. 102 (2019) 1628–1641,

[22] Y. He, R. Xu, S. He, H. Chen, K. Li, Y. Zhu, Q. Shen, An investigation of the NO3- concentration effect on lead anodic electrochemical behavior in NaOH solution, Int. J. Electrochem. Sci. 12 (2017) 9697 – 9713.

[23] Q.Z. Zhao, J.R.Qiu, X.W. Jiang, C.Z. Zhao, C.S. Zhu, Mechanisms of the refractive index change in femtosecond laser−irradiated Au^{3+}-doped silicate glasses. J. Appl. Phys. 96 (2004) 7122–7125.

[24] P. Juste, I.P. Santos, L.M.L Marzán, P. Mulvaney, Gold nanorods: synthesis characterization and applications, Coord. Chem. Rev. 249 (2005) 1870–1901

[25] U. Kreibig, C.V. Fragstein, The limitation of electron mean free path in small silver particles. J. Phys. A 224 (1969) 307–323.

[26] T. Hayakawa, S. Tamil Selva, M. Nogami, Field enhancement effect of small Ag particles on the fluorescence from Eu^{3+} doped SiO_2 glass. Appl. Phys. Lett. 74 (1999) 1513–1515.

[27] K.J. Rao, Structural Chemistry of Glasses, Elsevier, Amsterdam, 2002.

[28] K. Srilatha, L. Pavic, A. Mogus-Milankovic, Ch. SrinivasaRao, G. Little Flower, V. Ravi Kumar, N. Veeraiah, The role of vanadium valence states and coordination on electrical conduction in lithium iodide borate glasses mixed with small concentration of silver iodide, J. Non-Cryst. Solids 357 (2011) 3538-3547.

[29] L.S. Rao, M.S. Reddy, D.K. Rao, N. Veeraiah, Influence of redox behavior of copper ions on dielectric and spectroscopic properties of Li_2O-MoO_3-B_2O_3:CuO glass system, Solid State Sci. 11 (2009) 578-587.

[30] C.J.F. Bottcher and P. Bordewijk, Theory of Electrical Polarization, Elsevier, Amsterdam, 1978.

[31] J. Ashok, N. Purnachand, J. Suresh Kumar, M. Srinivasa Reddy, B. Suresh, M.P.F. Graça, N. Veeraiah, Studies on dielectric dispersion, relaxation kinetics and a.c. conductivity of Na_2O−CuO−SiO_2 glasses mixed with different concentrations of Bi_2O_3-Influence of redox behaviour of copper ions, J. Alloys Compd. 696 (2017) 1260−1268.

[32] C. Filipicˇ, A. Mogus-Milankovic´, L. Pavic´, K. Srilatha, N. Veeraiah, Polaronic behavior of MnO doped LiI-AgI-B_2O_3 glass, J. Appl. Phys. 112 (2012) 073705.

[33] A. Moguš-Milanković, L. Pavić, K. Srilatha, Ch. Srinivasa Rao, T. Srikumar, Y. Gandhi and N. Veeraiah, Electrical, dielectric and spectroscopic studies on MnO doped LiI-AgI-B_2O_3 glasses, J. Appl. Phys. 111 (2012) 013714.

[34] G. Austin and N.F. Mott, Polarons in crystalline and non-crystalline materials, Adv. Phys. 50 (2001) 757-812

Caption for Tables

Table 1 Physical parameters of the Li_2O-Pb_3O_4-SiO_2: Au_2O_3 glasses

Table 2 Summary of the data on differential thermal analysis studies

Table 3 Summary of the data on optical absorption spectra of Li_2O−Pb_3O_4−SiO_2:Au_2O_3 glasses.

Table 4 Summary of the data of band positions (in cm^{-1}) of various structural units in FT–IR spectra of Li_2O− Pb_3O_4−SiO_2:Au_2O_3 glasses. The values of the peak positions were measured to a precision of ±1 cm^{-1}.

Table 5 Summary of the data on a.c. conductivity and other parameters of Au_2O_3 doped Li_2O−Pb_3O_4−SiO_2 glasses.

Caption for Figures

Fig. 1 An illustration of (a) holodirected (b) hemidirected coordination of lead ions

Fig. 2 Photographs of the heat treated Li_2O-Pb_3O_4-SiO_2 glasses doped with different concentrations of Au_2O_3.

Fig. 3 XRD profiles of heat treated Li_2O-Pb_3O_4-SiO_2 glasses doped with different concentrations of Au_2O_3.

Fig. 4 SEM images of heat treated Li_2O-Pb_3O_4-SiO_2 glasses doped with different concentrations of Au_2O_3. The figure also consists of EDS for the glass Au_8.

Fig. 5 (a) Deconvoluted and fitted XPS spectra of Au^0 and Au^{3+} ions in the glass samples Au_1 and Au_4. Inset represents the variation of the intensity of the peaks connected with Au^0 metallic particles and Au^{3+} ions with the concentration of Au_2O_3.

Fig. 5 (b) Deconvoluted and fitted XPS spectra of PbO, PbO_2 and Pb_3O_4 in the glass sample Au_2 and inset represents the intensity variation of the peaks related to PbO_2 and Pb_3O_4 ($4f_{7/2}$) with the concentration of gold oxide

Fig. 6 DTA traces of heat treated Li_2O-Pb_3O_4-SiO_2 glasses doped with different concentrations of Au_2O_3.

Fig. 7(a) Optical absorption spectra of Li_2O-Pb_3O_4-SiO_2 glasses doped with different concentrations of Au_2O_3 recorded after heat treatment.

Fig. 7(b) Tauc plots of heat treated Li_2O-Pb_3O_4-SiO_2 glasses doped with different concentrations of Au_2O_3. Inset represents the variation of E_o with concentration of Au_2O_3.

Fig. 8 IR spectra of heat treated Li_2O-Pb_3O_4-SiO_2 glasses doped with different concentrations of Au_2O_3.

Fig. 9 Variation of dielectric constant (a) with frequency measured at different temperatures for the sample Au_1 and (b) with temperature measured at different frequencies for the sample Au_2. Inset represents the variation of ε' (ω) with the concentration of Au_2O_3 measured at 250 °C and 1kHz.

Fig. 10 Variation of dielectric loss (a) with frequency measured at different temperatures and (b) with temperature measured at different frequencies for the sample Au_8

Fig. 11 Variation of electric moduli M' and M'' (a) with frequency at different temperatures for the sample Au_2 (b) with temperature at different frequencies for the sample Au_8

Fig. 12 The plots of relaxation time *vs* temperature for Li_2O-Pb_3O_4-SiO_2glasses doped with different concentrations of Au_2O_3.Inset represents the variations of τ evaluated at 470 K with the concentration of Au_2O_3.

Fig. 13 Cole-Cole plots forLi_2O-Pb_3O_4-SiO_2 glasses doped with different concentrations of Au_2O_3 drawn in the temperature range of 200-250 ^oC.

Fig. 14 Variation of (a) Z' and (b) Z" with frequency at different temperatures for the sample Au_4

Fig. 15 The plots of Z' vs Z" drawn in the temperature regions (a) 30 - 50 ^oC (b) 90 - 110 ^oC (c) 125 - 150 ^oC (d) 225 - 250 ^oC for the sample Au_1.

Fig. 15 (e) The comparison plots of impedance of Li_2O-Pb_3O_4-SiO_2 glasses doped with different concentrations of Au_2O_3 drawn at 250 ^oC. In the equivalent circuit diagram the parallel CR circuit accounts for semi-circular path of the diagram, whereas additional series capacitor represents the inclined spur part in the diagram.

Fig. 15(f) Bode plots (plots of total impedance |Z| and the phase angle, φ= arc tan(Z″/Z′) *vs* ω) for a selected glass sample Au_2 drawn at 200 °C.

Fig. 16 The plots of σ_{ac}(a) *vs* frequency drawn at different temperatures (b) *vs* 1/T drawn at different frequencies for the glass sample Au_6. Inset represents the variation of σ_{ac} with the concentration of Au_2O_3 measured at 250 ^oC and 1kHz

Fig. 17 Plots of log $\sigma_{ac}(\omega)$ versus log ω for the glass sample Au_6 drawn at different temperatures to evaluate frequency exponent. Inset represents the variation of s with the temperature

Table 1

Physical parameters of the Li_2O-Pb_3O_4-SiO_2: Au_2O_3 glasses

Glass	Conc. Au_2O_3 (mol%)	Density d (g/cm^3) (±0.001)	Gold ion conc. N_i(x10^{18}/cm^3) (±0.01)	Interionic distance of Gold ions R_i (Å)(±0.01)	Polaron radius R_p(Å) (±0.01)
Au_1	0.01	4.368	2.379	7.49	3.01
Au_2	0.02	4.502	4.902	5.88	2.37
Au_4	0.04	4.505	9.802	4.67	1.88
Au_6	0.06	4.511	14.71	4.08	1.64
Au_8	0.08	4.533	19.70	3.70	1.49

Table 2
Summary of the data on differential thermal analysis studies

Glass	Glass transition temperature T_g (±1 °C)	Crystallization temperature T_{c1} (±1 °C)	T_{c1}-T_g(±1 °C)
Au_1	379	526	147
Au_2	380	513	133
Au_4	390	543	153
Au_6	381	525	144
Au_8	384	522	138

Table 3

Summary of the data on optical absorption spectra of $Li_2O–Pb_3O_4–SiO_2:Au_2O_3$ glasses.

Absorption Band details → Glass ↓	Au_1	Au_2	Au_4	Au_6	Au_8
SPR band position(nm)	527.6	523	516	522	525
Cut-off wavelength (nm)	322	316	283	295	306
Optical bandgapE_o (eV)	3.19	3.40	3.82	3.69	3.54
Size of the Au^0 particles (nm)	5.13	4.93	3.04	5.43	5.56

Table 4

Summary of the data of band positions (in cm^{-1}) of various structural units in FT–IR spectra of $Li_2O–Pb_3O_4–SiO_2:Au_2O_3$glasses. The values of the peak positions are measured to a precision of ± 1 cm^{-1}.

Glass	Asymmetric stretching vibrations of O-Si-Obonds	Symmetric stretching vibrations of SiO_4 units	Pb(IV)-O bond	PbO_4 units
Au_1	998	772	579	463
Au_2	1019	769	575	460
Au_4	1032	766	570	456
Au_6	1028	768	572	459
Au_8	1022	771	576	461

Table 5

Summary of the data on a.c. conductivity and other parameters of Au_2O_3 doped $Li_2O{-}Pb_3O_4{-}SiO_2$ glasses.

Glass	Exponent s (± 0.01)	$N(E_F)$ (x 10^{21}, eV^{-1}/cm^3) (± 0.01)	A.E. for conduction W_{ac} (eV) (±0.01)	A.E. for dipoles (eV) (± 0.01)	Spreading factor (rads) α' (± 0.01)
Au_1	0.36	2.08	0.65	0.29	0.90
Au_2	0.42	1.98	0.72	0.32	0.81
Au_4	0.48	1.71	0.94	0.48	0.63
Au_6	0.43	1.78	0.84	0.41	0.68
Au_8	0.40	1.86	0.76	0.38	0.75

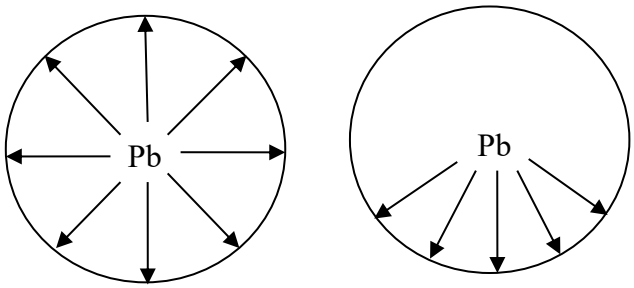

Fig. 1 An illustration of (a) holodirected (b) hemidirected coordination of lead ions

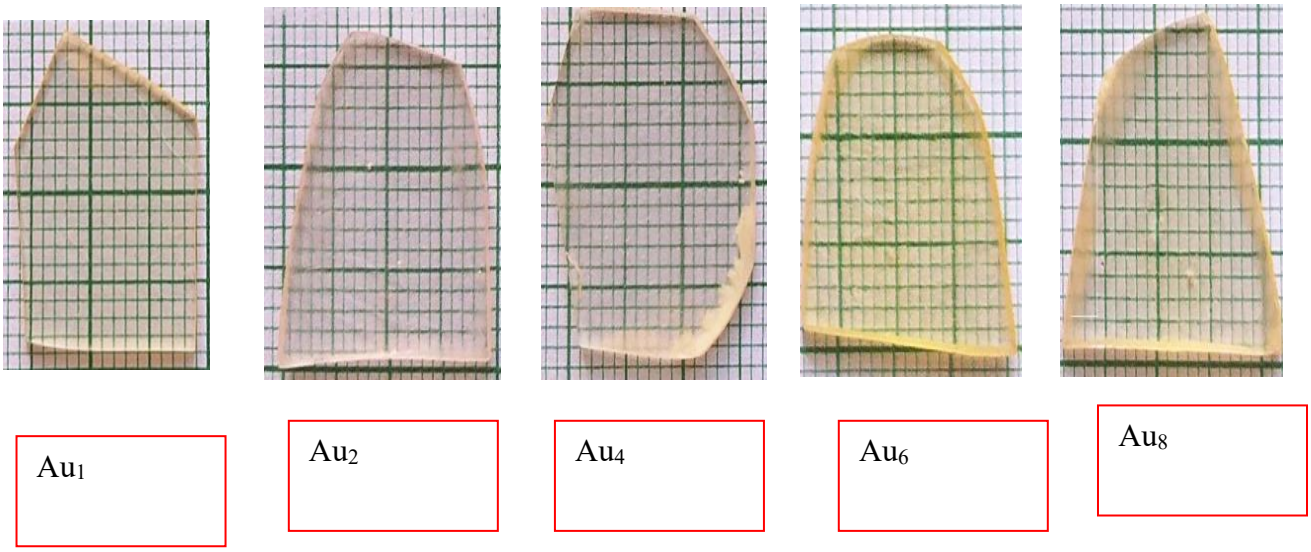

Fig. 2 Photographs of the heat-treated Li_2O-Pb_3O_4-SiO_2 glasses doped with different concentrations of Au_2O_3.

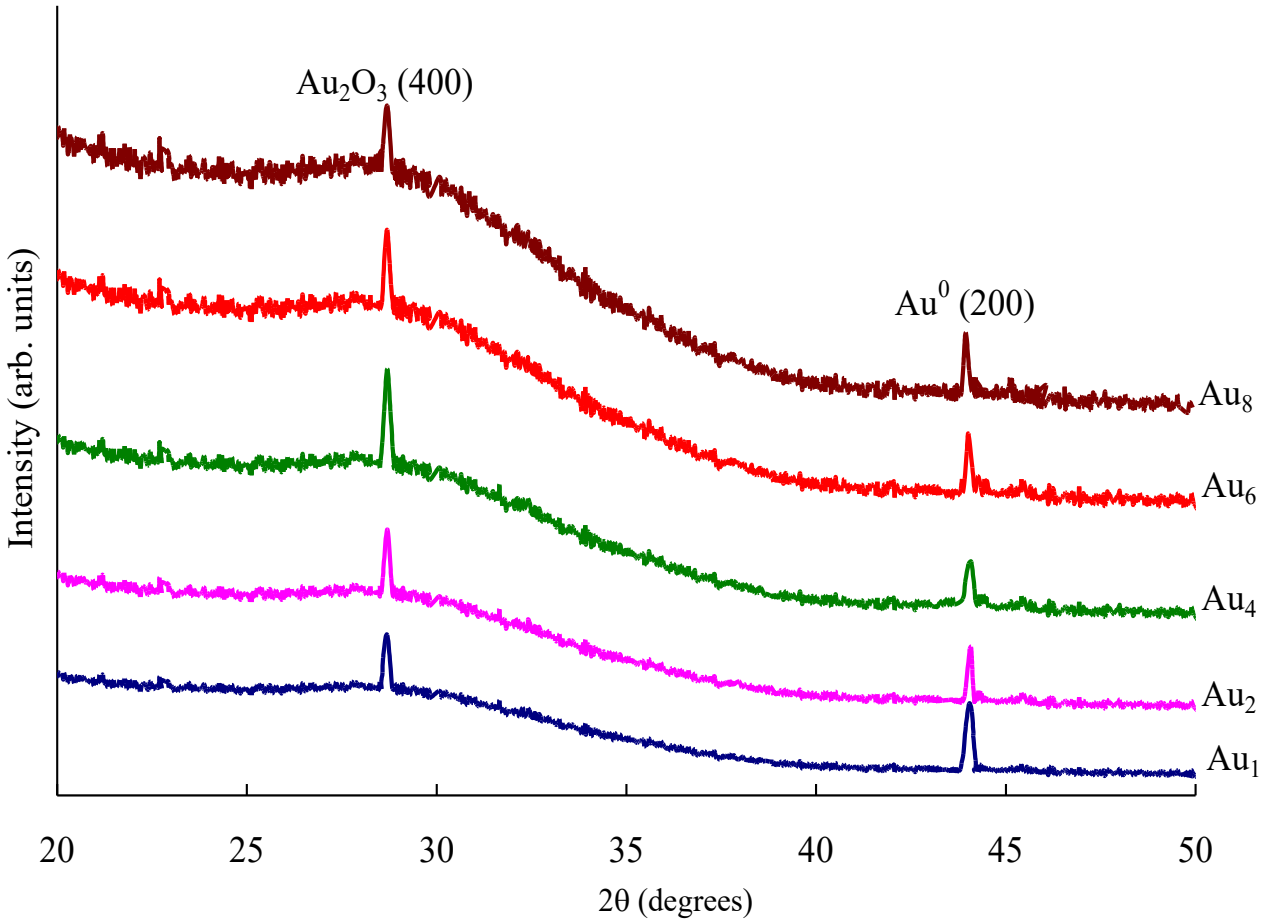

Fig. 3 XRD profiles of heat treated Li_2O-Pb_3O_4-SiO_2 glasses doped with different concentrations of Au_2O_3.

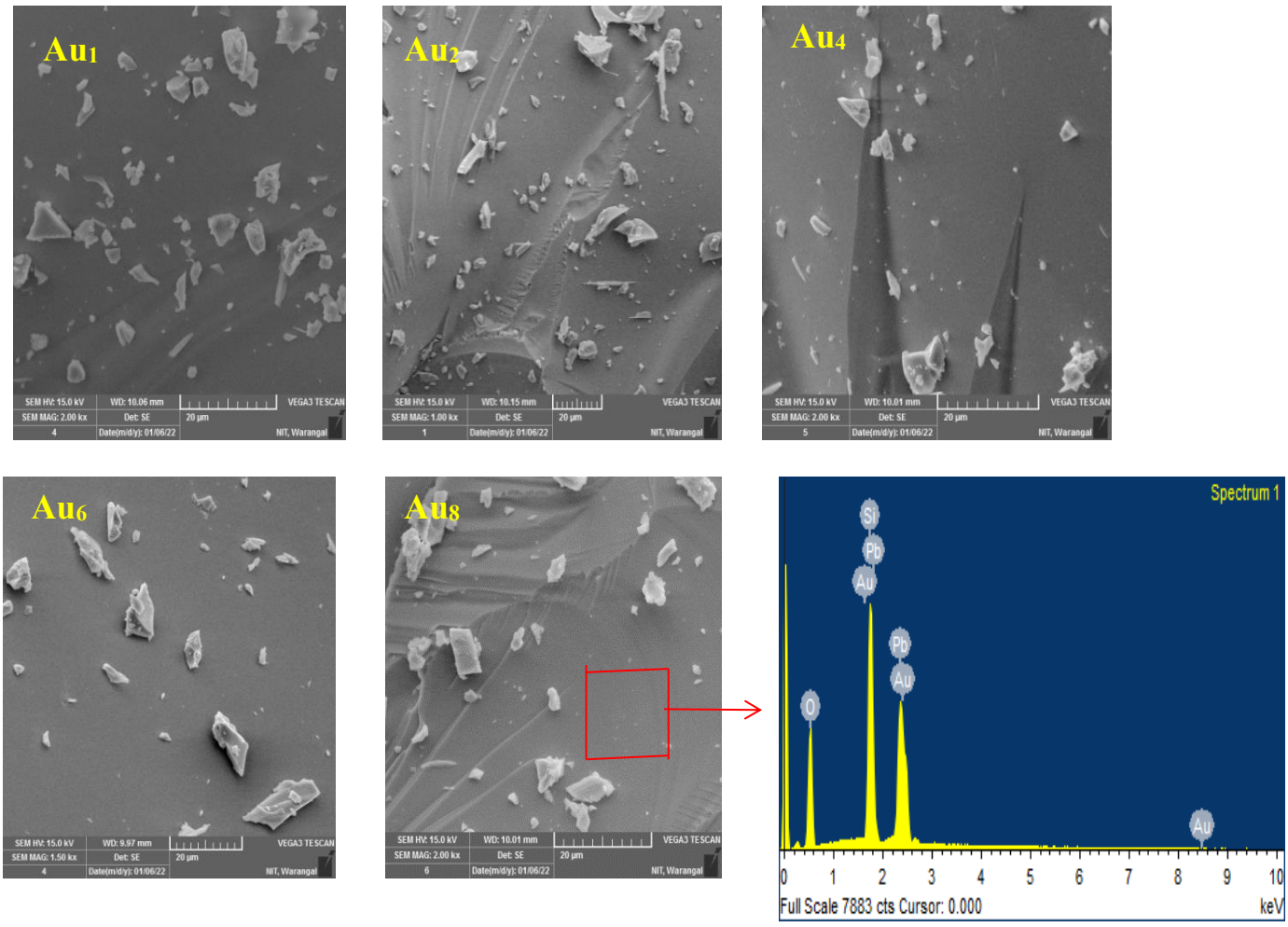

Fig. 4 SEM images of heat-treated Li_2O-Pb_3O_4-SiO_2 glasses doped with different concentrations of Au_2O_3. The figure also consists of EDS for the sample Au_8.

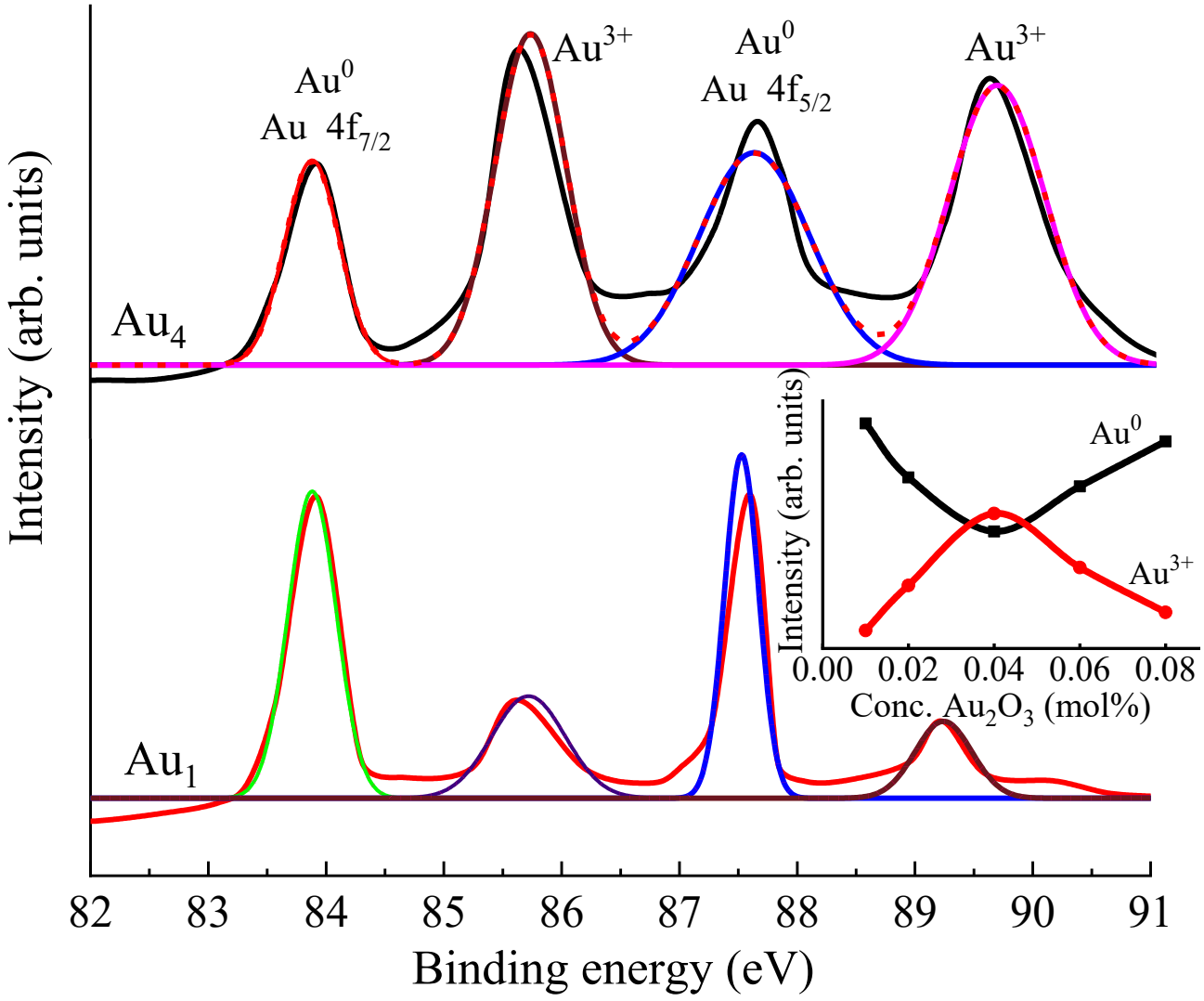

Fig. 5(a) Deconvoluted and fitted XPS spectra of Au^0 and Au^{3+} ions in the glass samples Au_1 and Au_4. Inset represents the variation of the intensity of the peaks connected with Au^0metallic particles and Au^{3+} ions with the concentration of Au_2O_3.

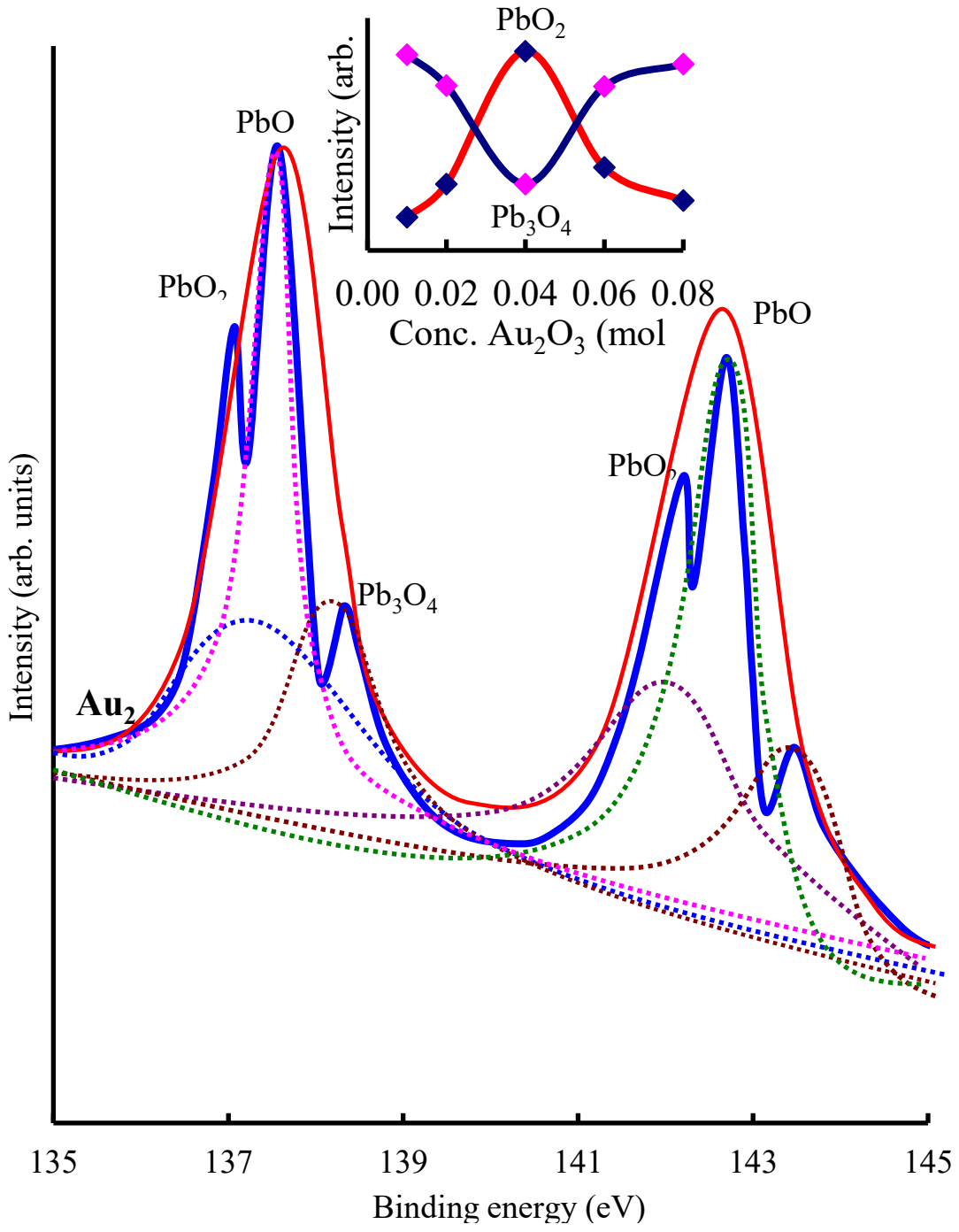

Fig. 5 (b) Deconvoluted and fitted XPS spectra of PbO, PbO_2 and Pb_3O_4 in the glass sample Au_2 and inset represents the intensity variation of PbO_2 and Pb_3O_4 ($4f_{7/2}$) with the concentration of gold oxide.

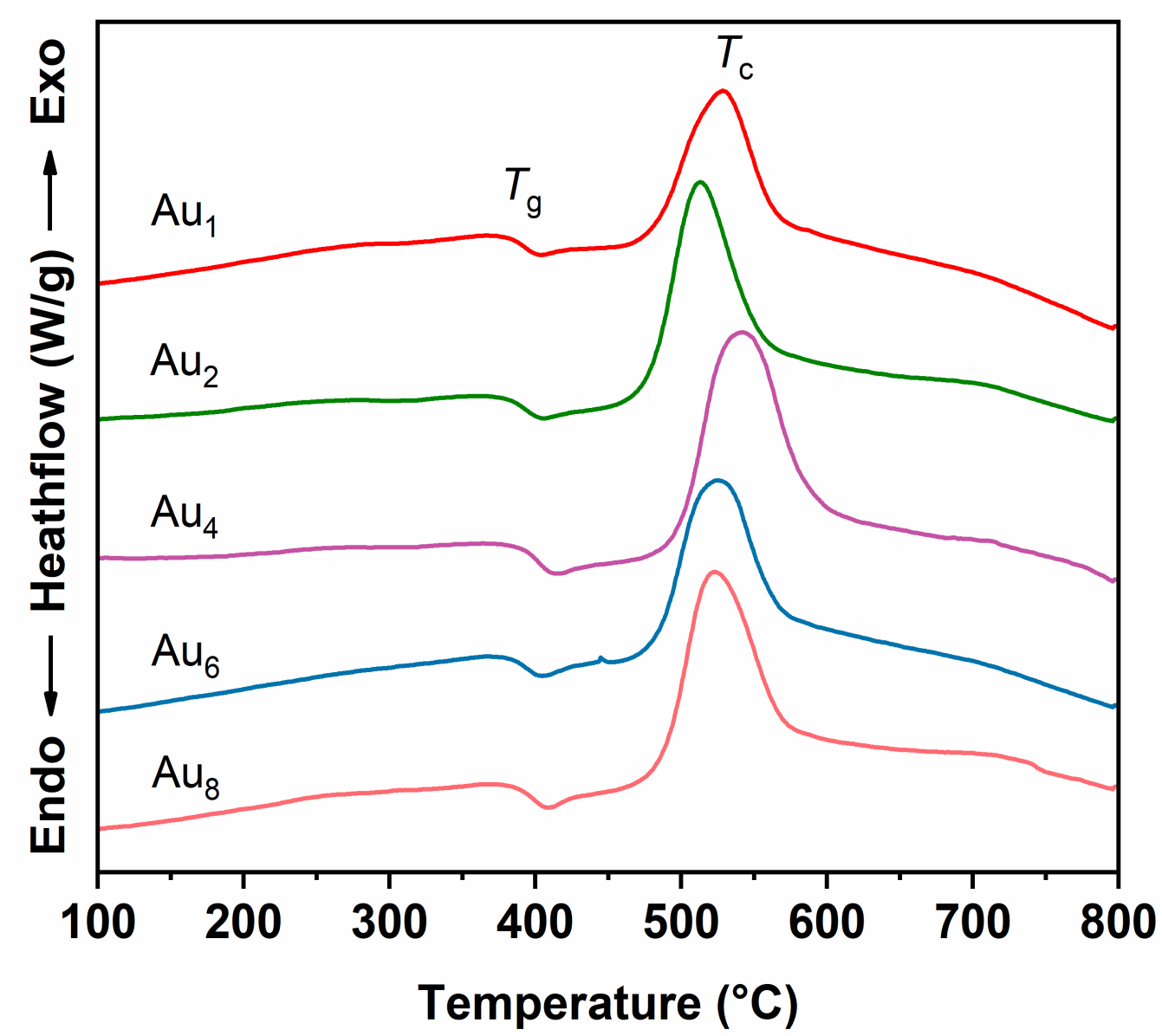

Fig. 6 DTA traces of heat-treated Li_2O-Pb_3O_4-SiO_2 glasses doped with different concentrations of Au_2O_3.

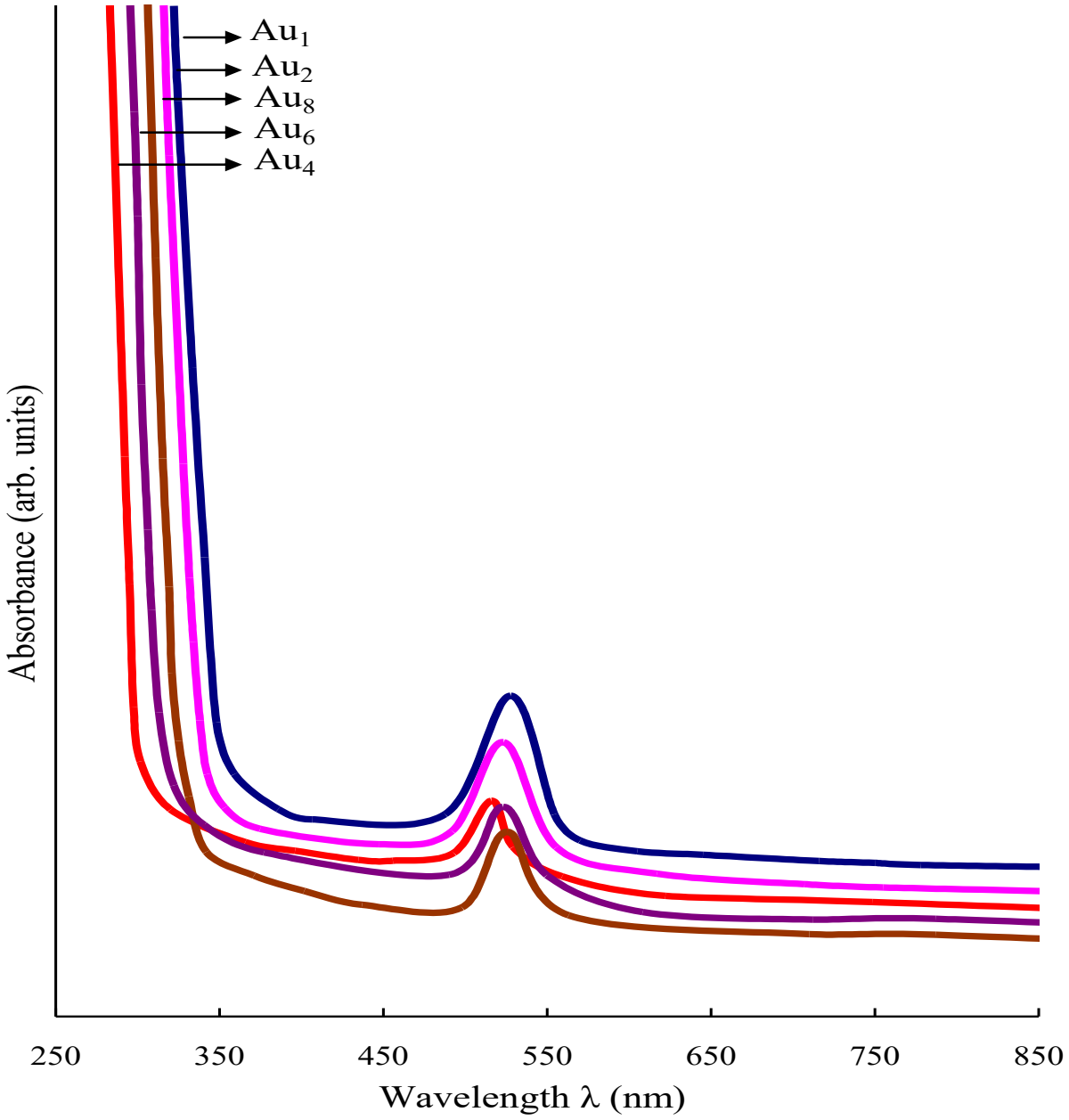

Fig. 7(a) Optical absorption spectra of Li_2O-Pb_3O_4-SiO_2 glasses doped with different concentrations of Au_2O_3 recorded after heat treatment.

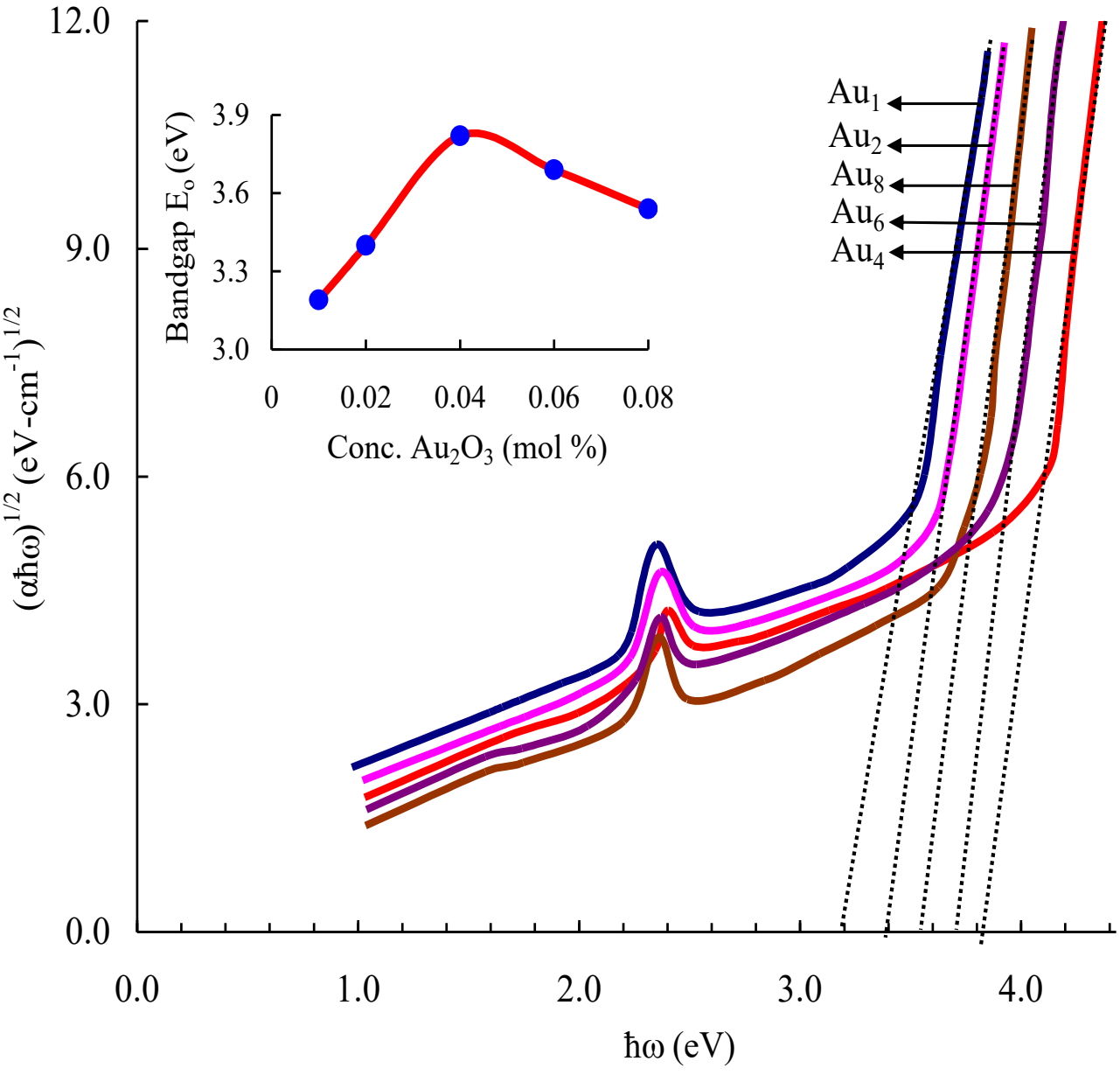

Fig. 7(b) Tauc plots of heat treated Li_2O-Pb_3O_4-SiO_2 glasses doped with different concentrations of Au_2O_3.Inset represents the variation of E_o with concentration of Au_2O_3.

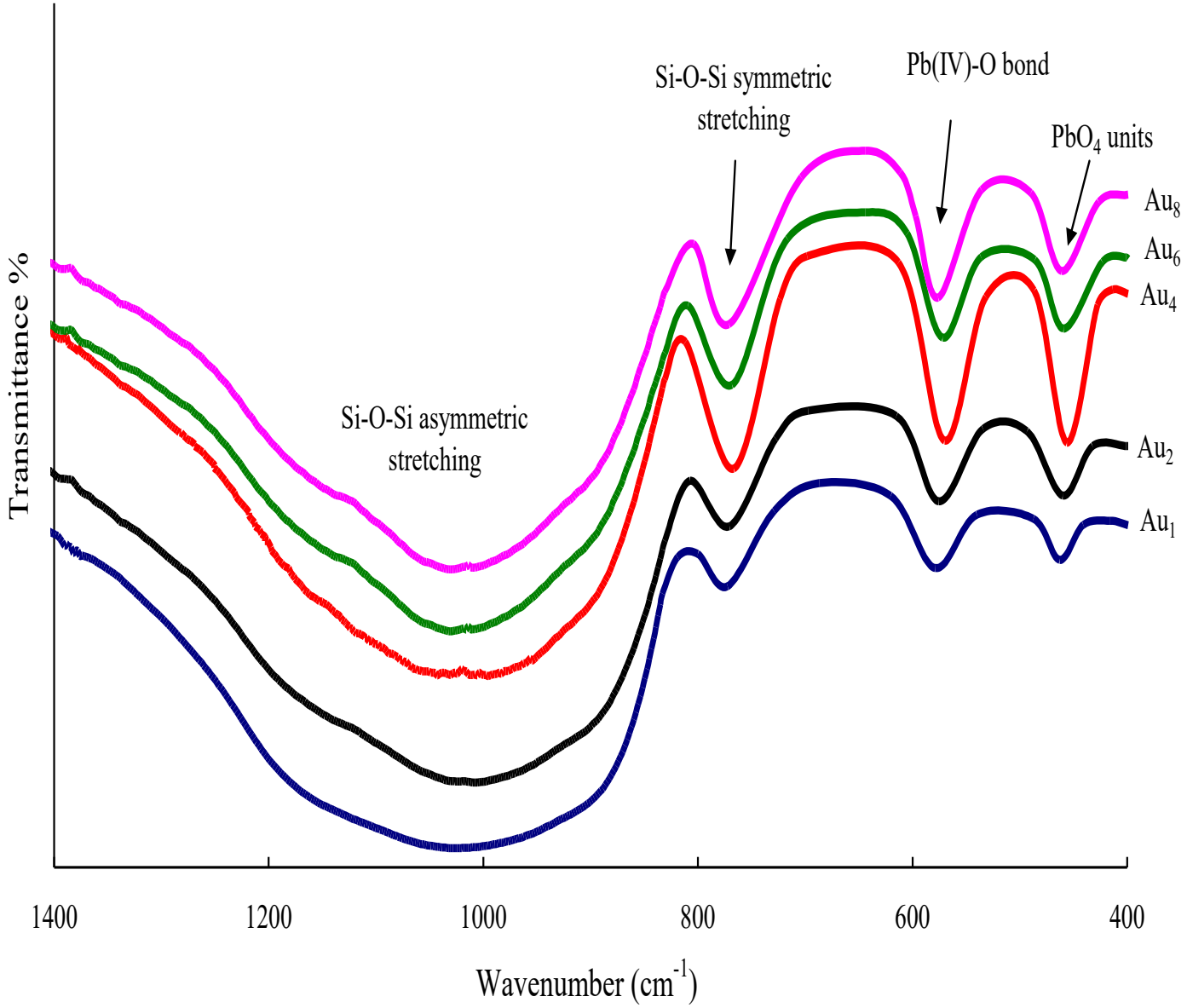

Fig. 8 FT-IR spectra of heat treated Li_2O-Pb_3O_4-SiO_2 glasses doped with different concentrations of Au_2O_3.

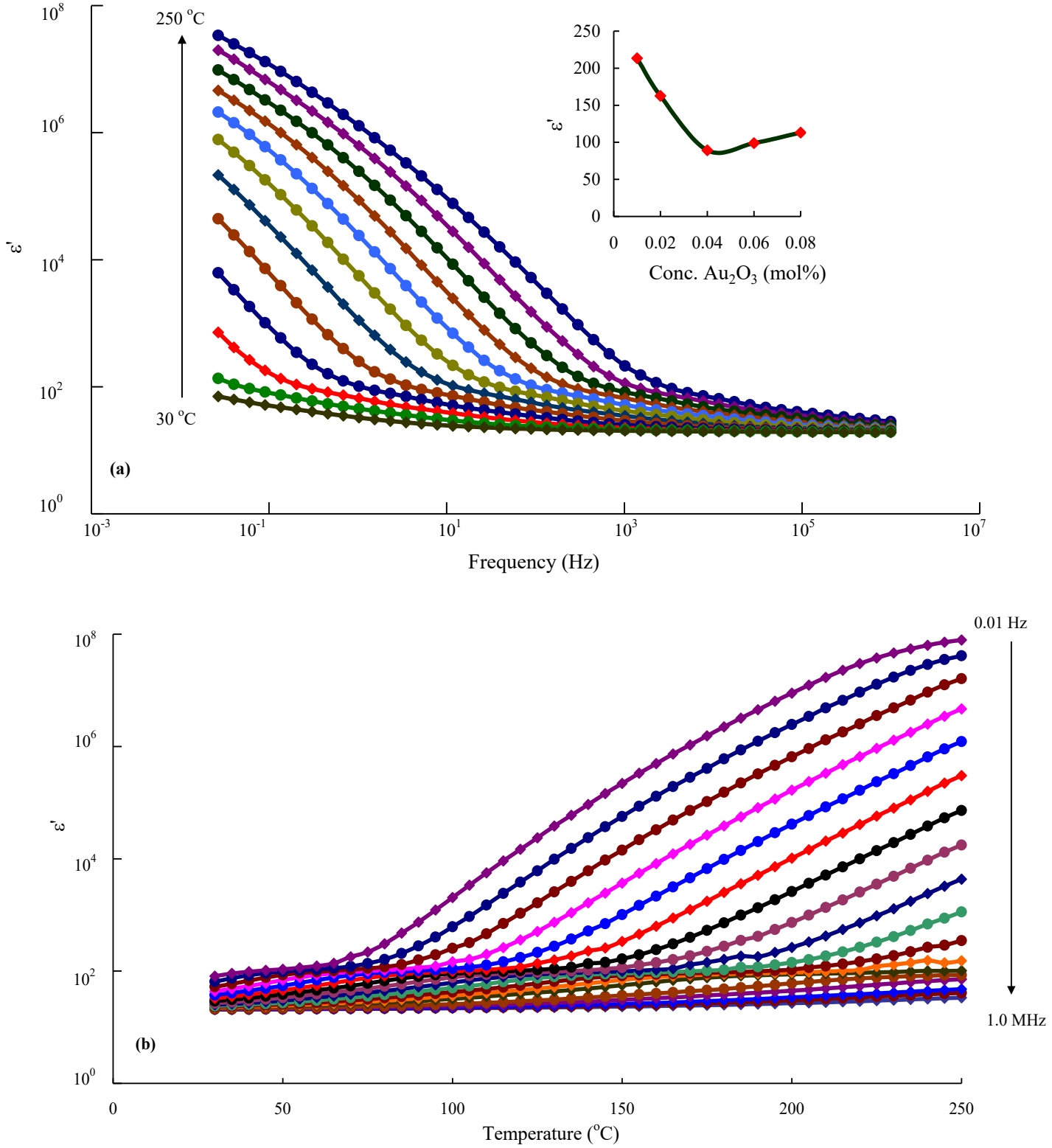

Fig. 9 Variation of dielectric constant (a) with frequency measured at different temperatures for the sample Au_1 and (b) with temperature measured at different frequencies for the sample Au_2. Inset represents the variation of ε' (ω) with the concentration of Au_2O_3 measured at 250 °C and 1 kHz.

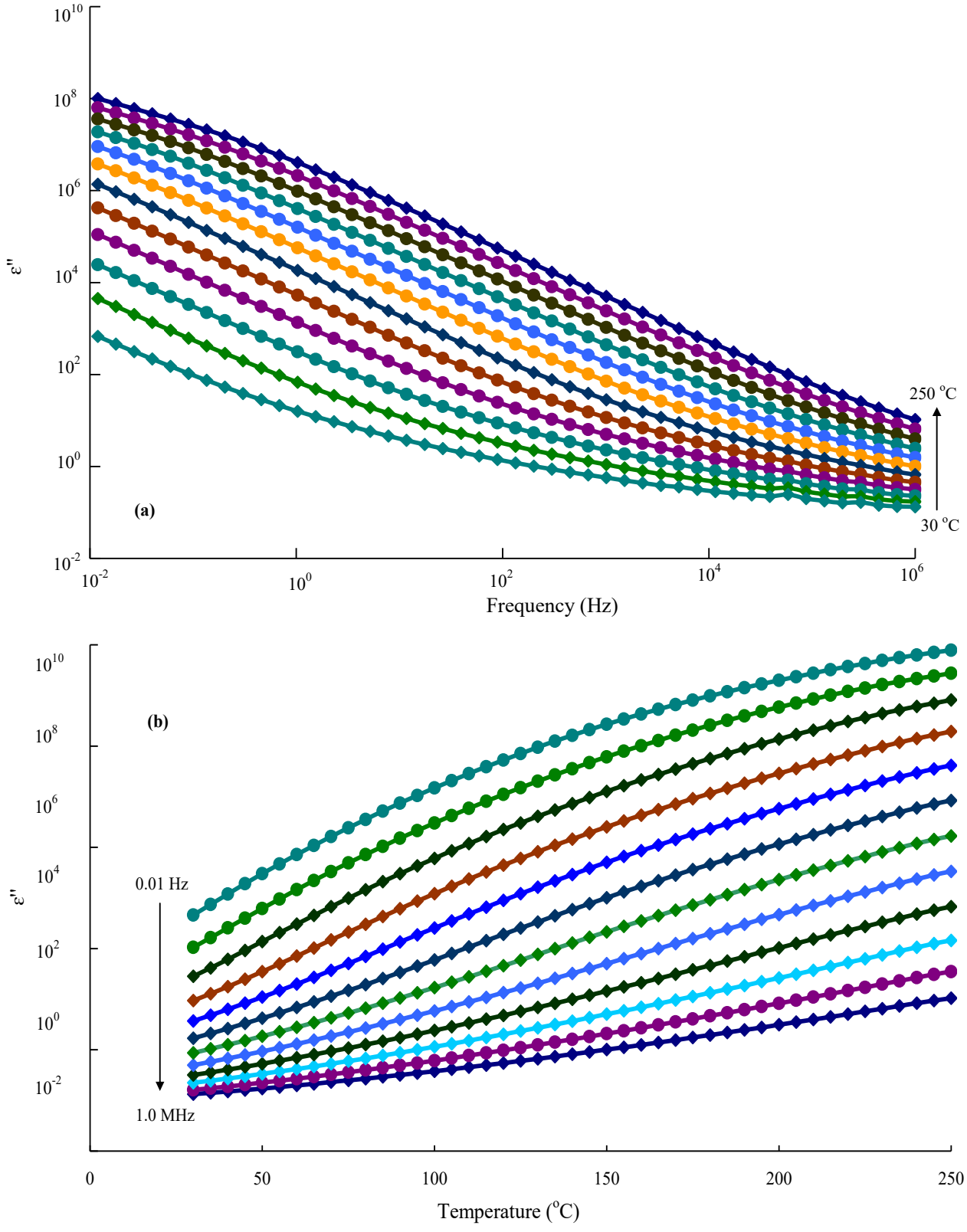

Fig. 10 Variation of ε″ (a) with frequency measured at different temperatures and (b) with temperature at different frequencies for the glass Au_8

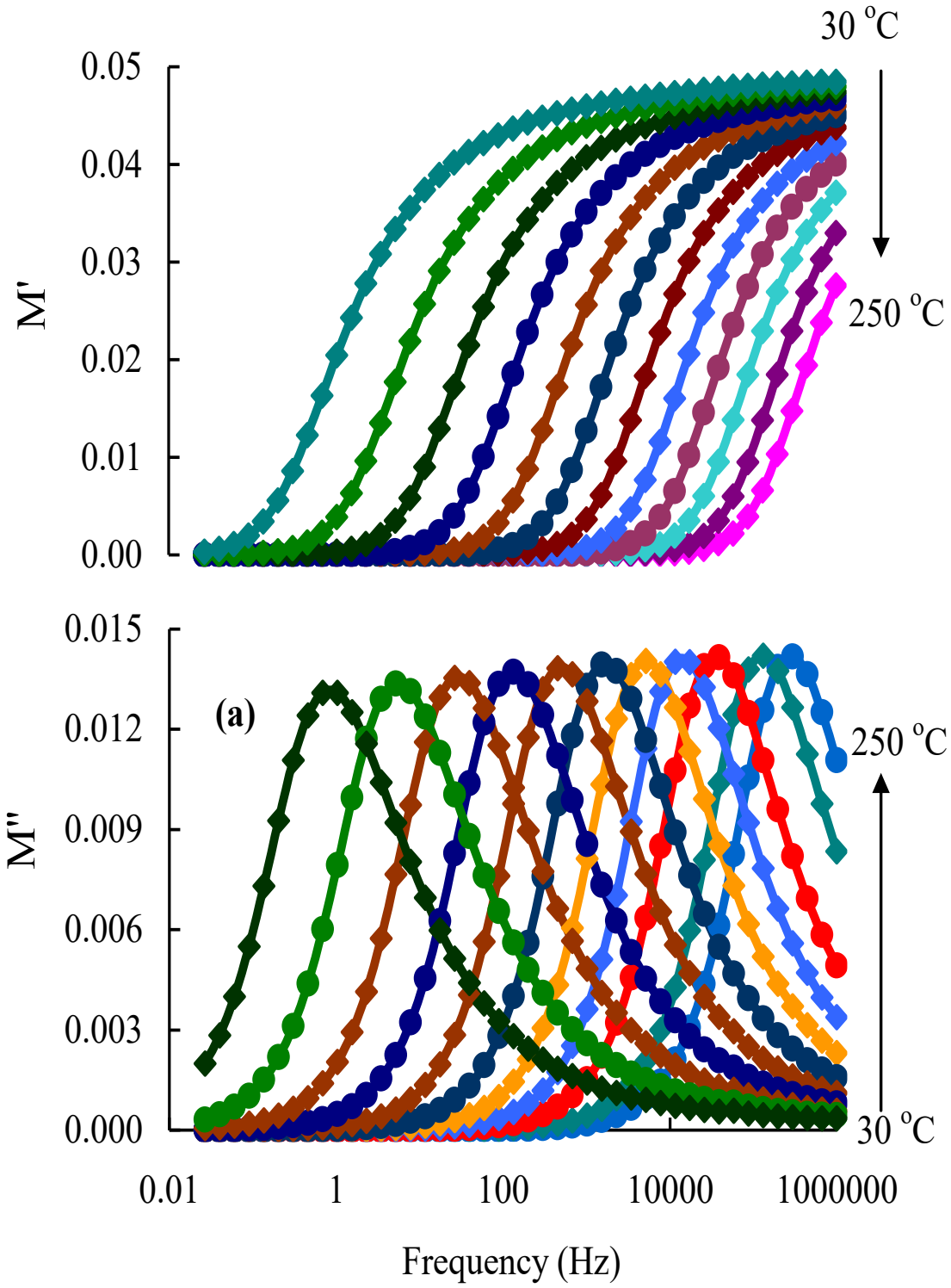
30 °C
250 °C
M'
0.05
0.04
0.03
0.02
0.01
0.00
(a)
M''
0.015
0.012
0.009
0.006
0.003
0.000
250 °C
30 °C
0.01
1
100
10000
1000000
Frequency (Hz)

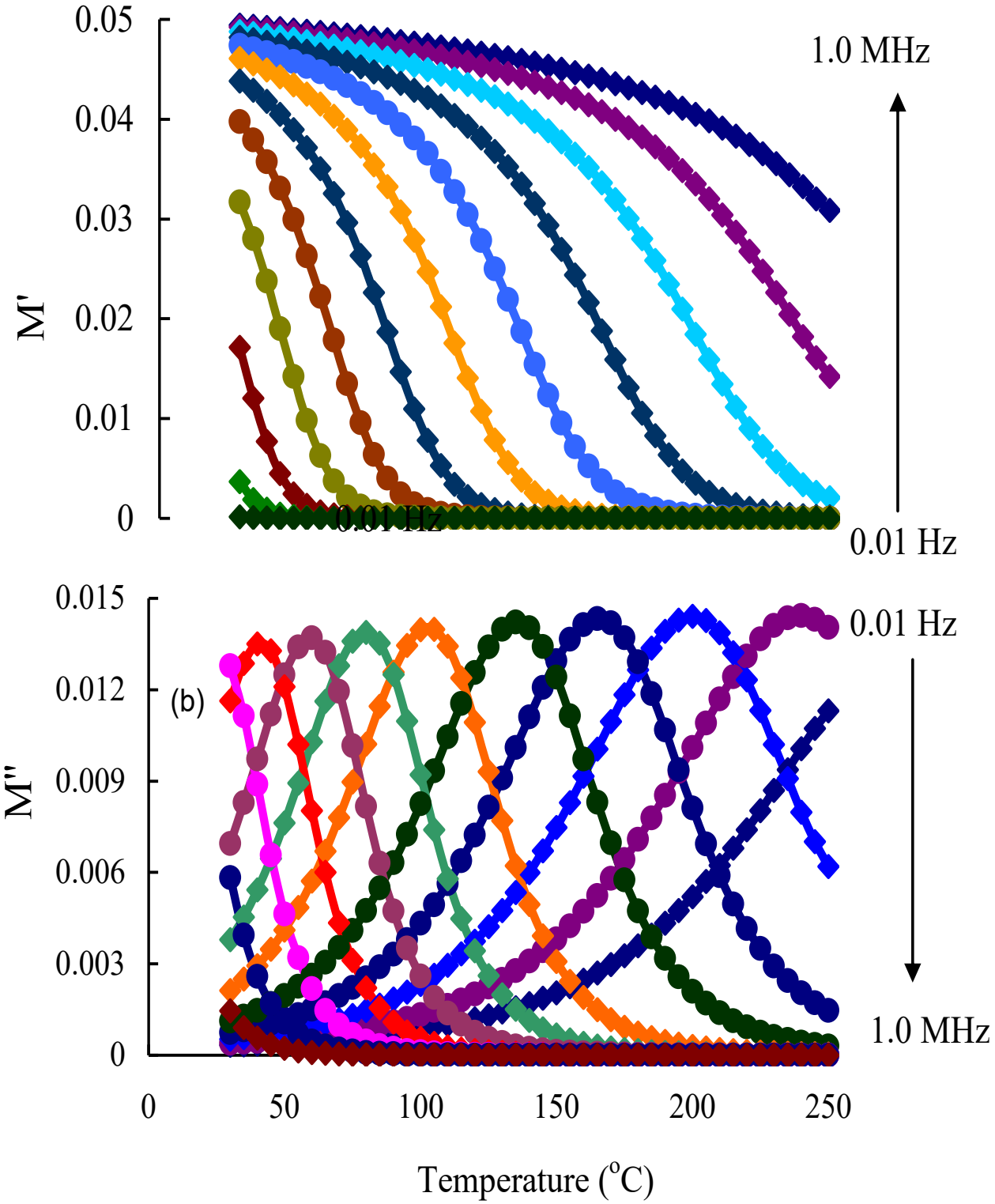

Fig. 11 Variation of electric moduli *M′* and *M″* (a) with frequency at different temperatures for the sample Au_2 (b) with temperature at different frequencies for the sample Au_8

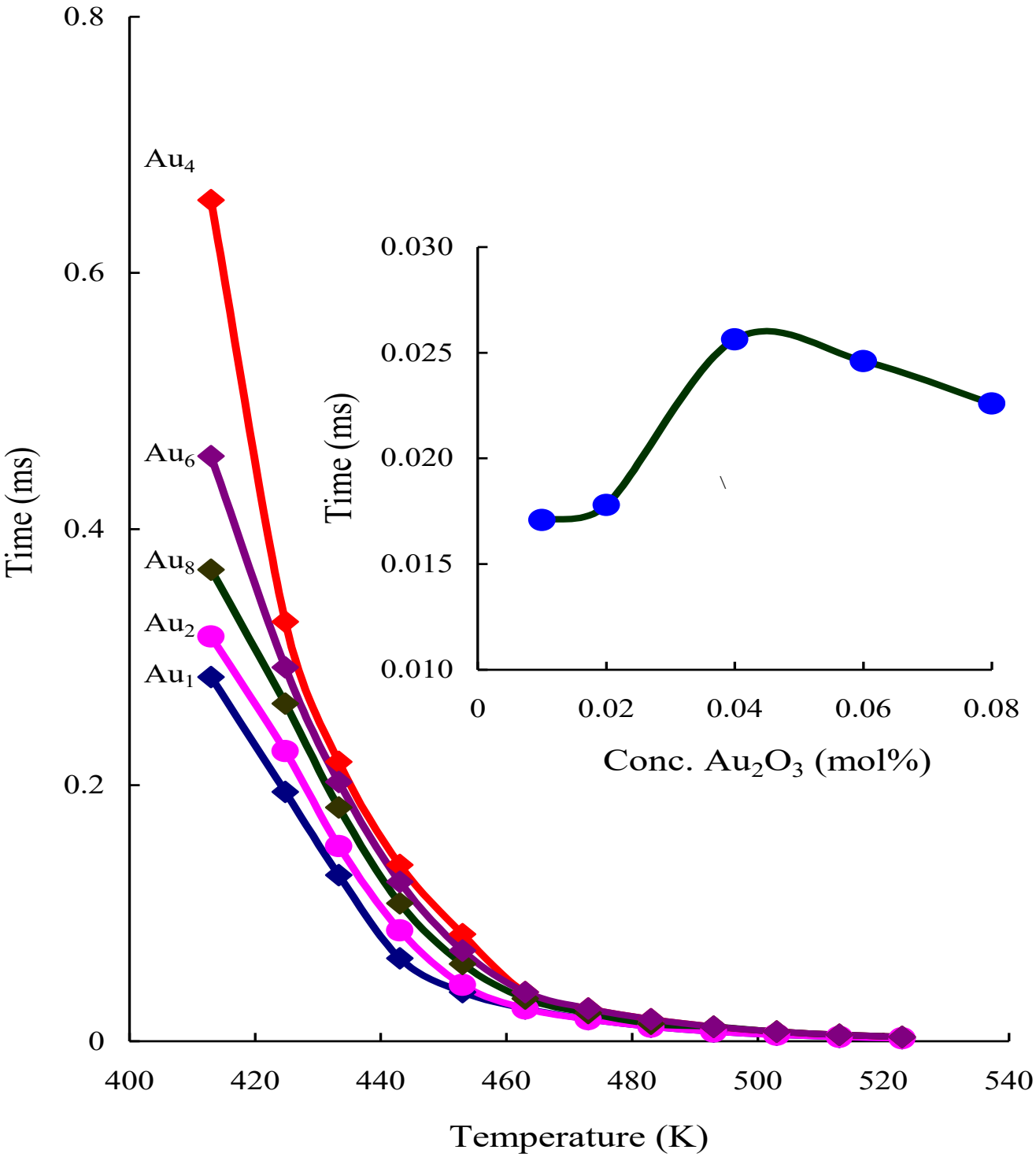

Fig. 12 The plots of relaxation times *vs* temperature for Li_2O-Pb_3O_4-SiO_2 glasses doped with different concentrations of Au_2O_3.Inset represents the variations of τ evaluated at 470 K with the concentration of Au_2O_3.

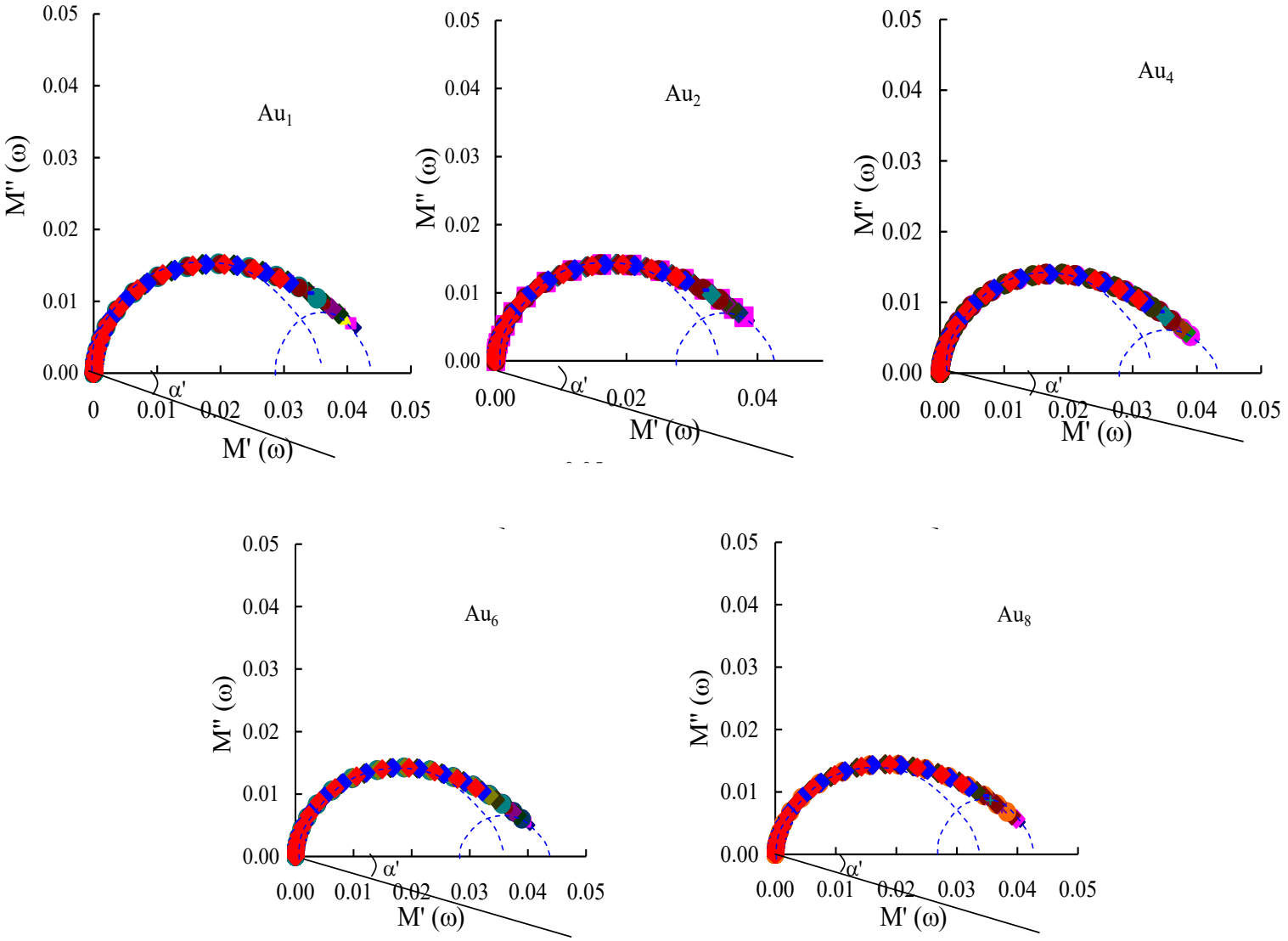

Fig. 13 Cole-Cole plots forLi_2O-Pb_3O_4-SiO_2 glasses doped with different concentrations of Au_2O_3drawn in the temperature range of 200-250 ºC.

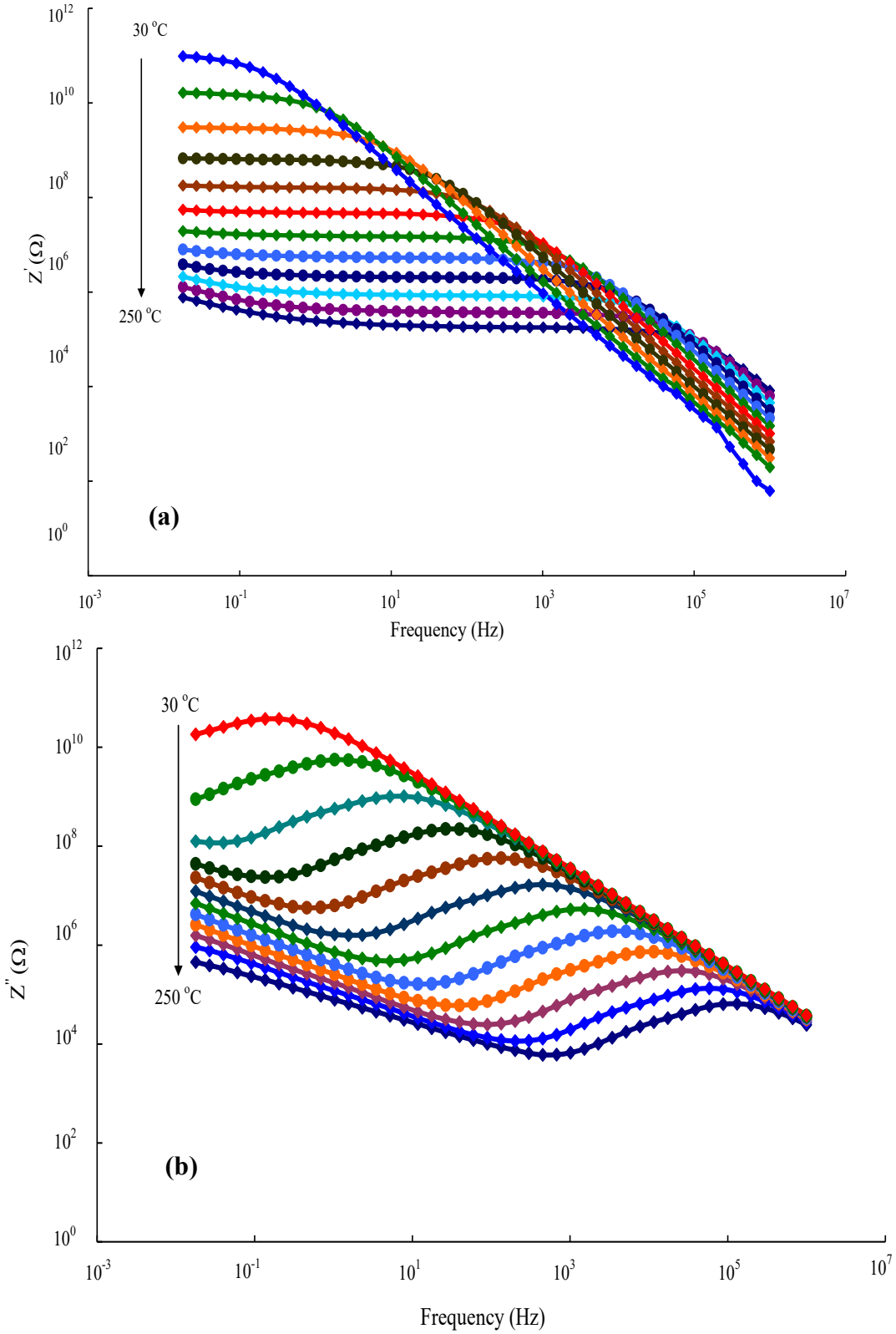

Fig. 14 Variation of (a) Z' and (b) Z'' with frequency at different temperatures for the sample Au_4

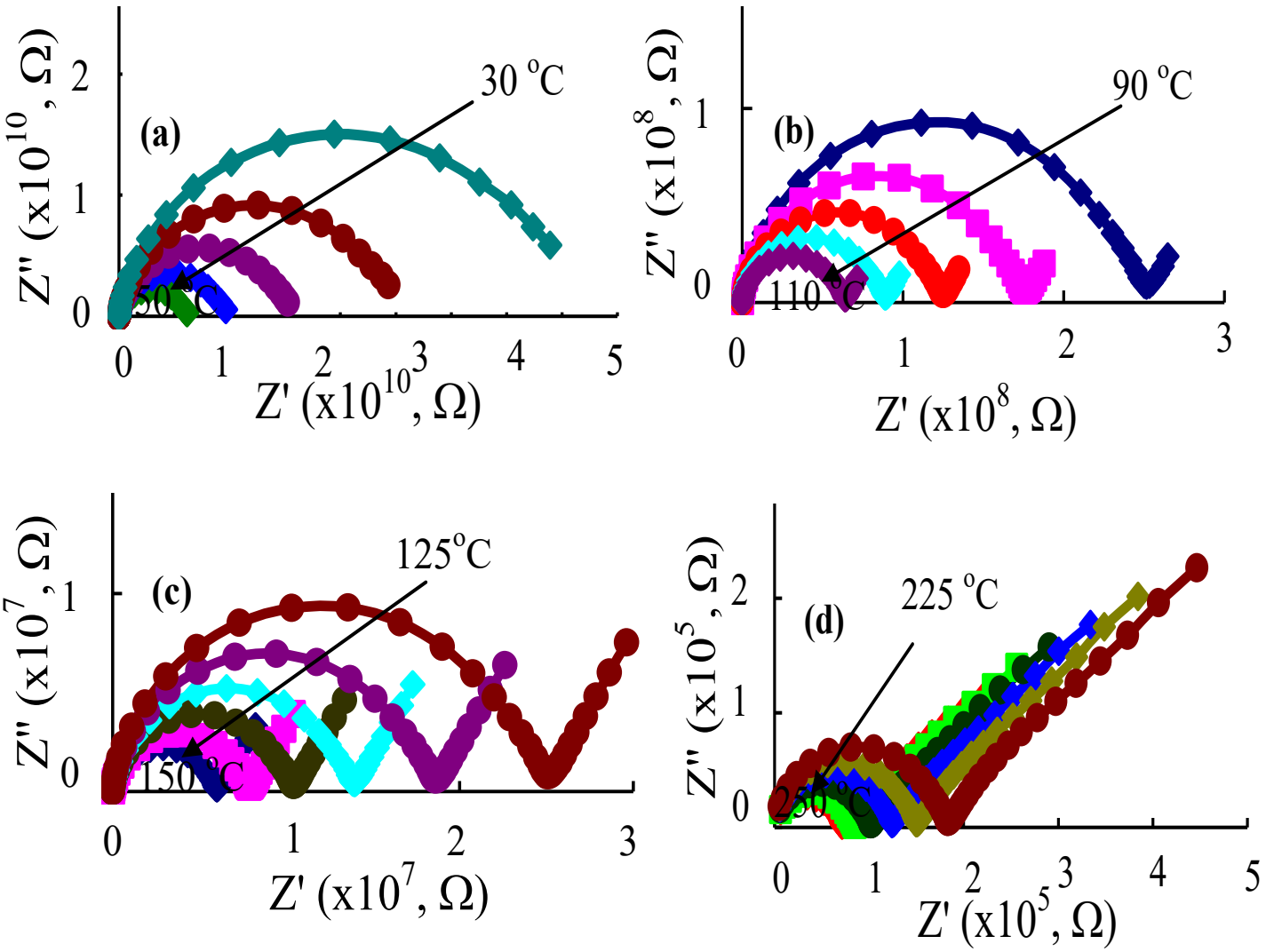

Fig.15 The plots of Z' vs Z'' drawn in the temperature regions (a) 30–50 ºC (b) 90–110 ºC (c) 125–150 ºC (d) 225–250 ºC for the sample Au_1.

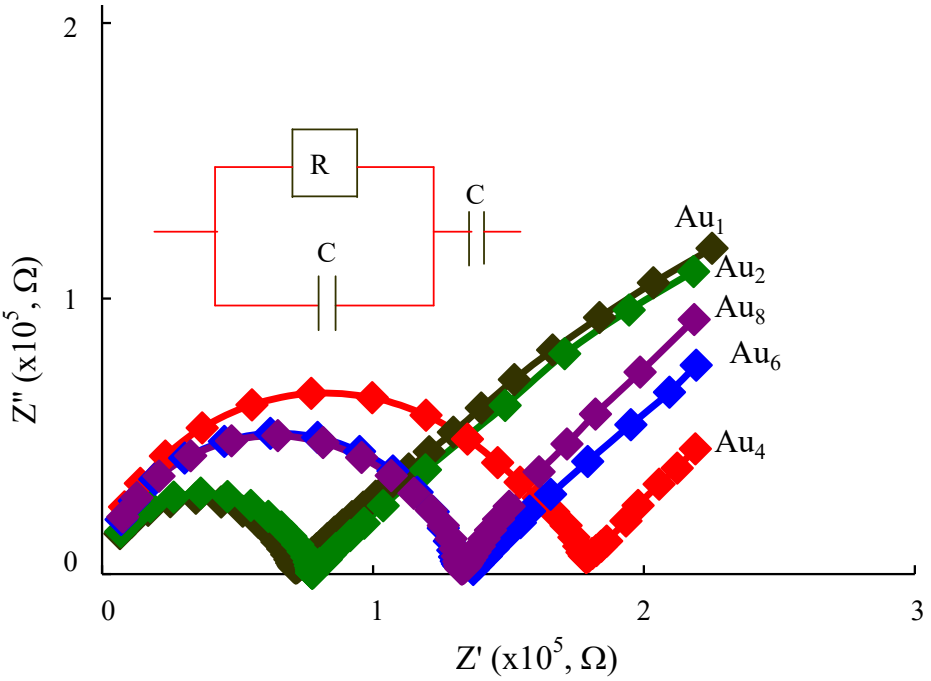

Fig.15 (e) The comparison plots of impedance of Li_2O-Pb_3O_4-SiO_2 glasses doped with different concentrations of Au_2O_3 drawn at 250 ºC. In the equivalent circuit diagram the parallel CR circuit accounts for semi-circular path of the diagram whereas additional series capacitor represents the inclined spur part in the diagram.

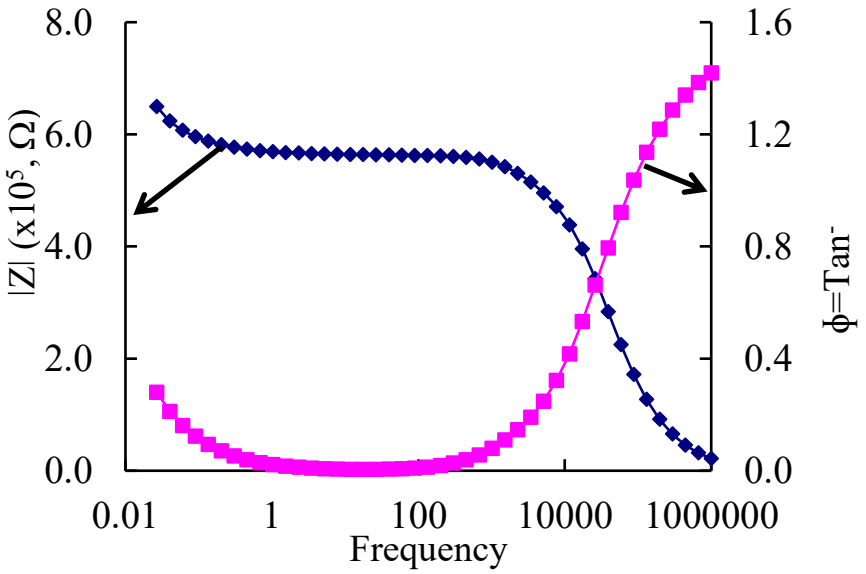

Fig. 15(f) Bode plots (plots of total impedance |Z| and the phase angle, $\varphi = \tan^{-1}(Z''/Z')$ vs ω) for a selected glass sample Au_2 drawn at 200 °C.

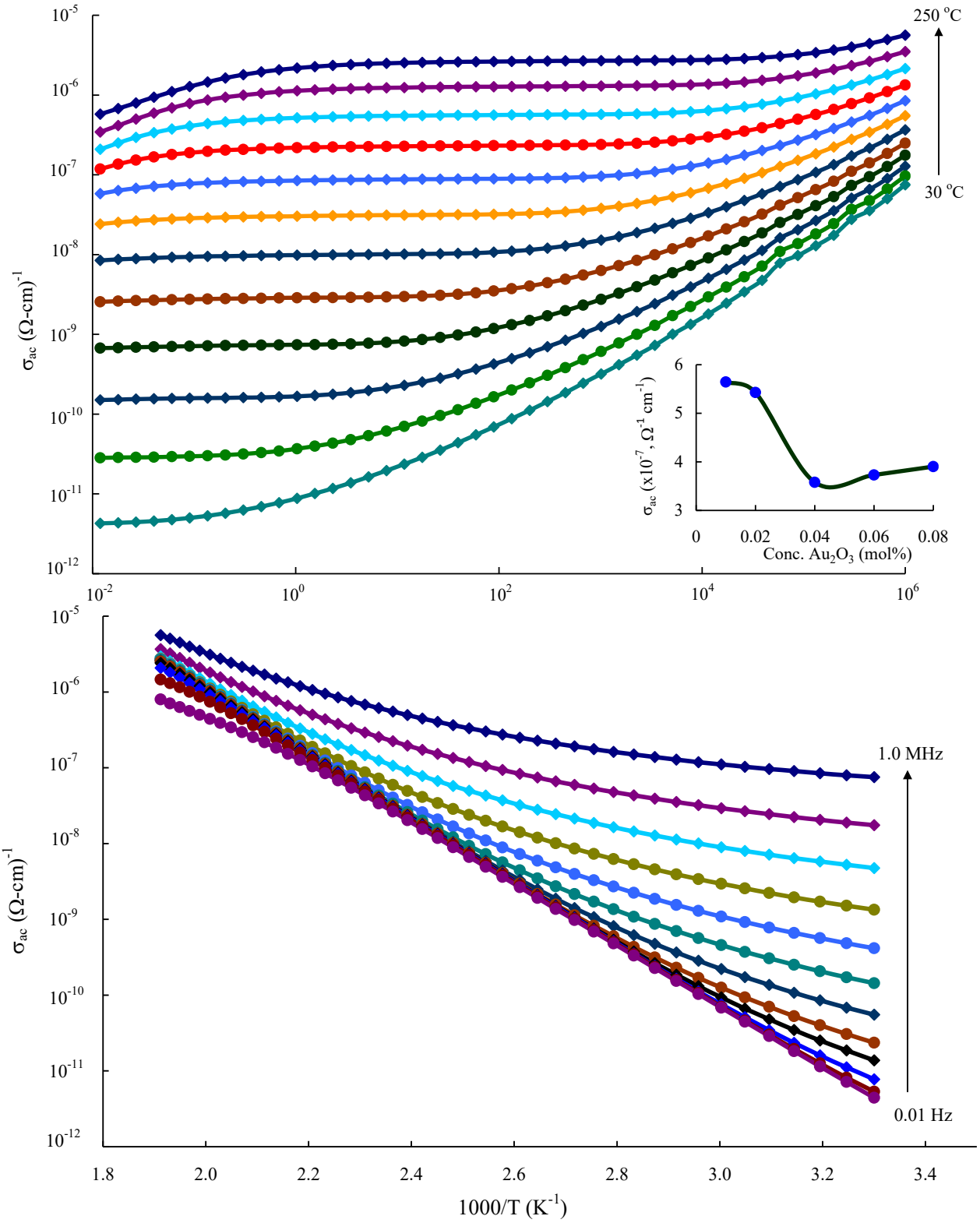

Fig. 16 The plots of σ_{ac} (a) *vs* frequency drawn at different temperatures (b) *vs 1/T* drawn at different frequencies for the glass sample Au_6. Inset represents the variation of σ_{ac} with the concentration of Au_2O_3 measured at 250 °C and 1kHz.

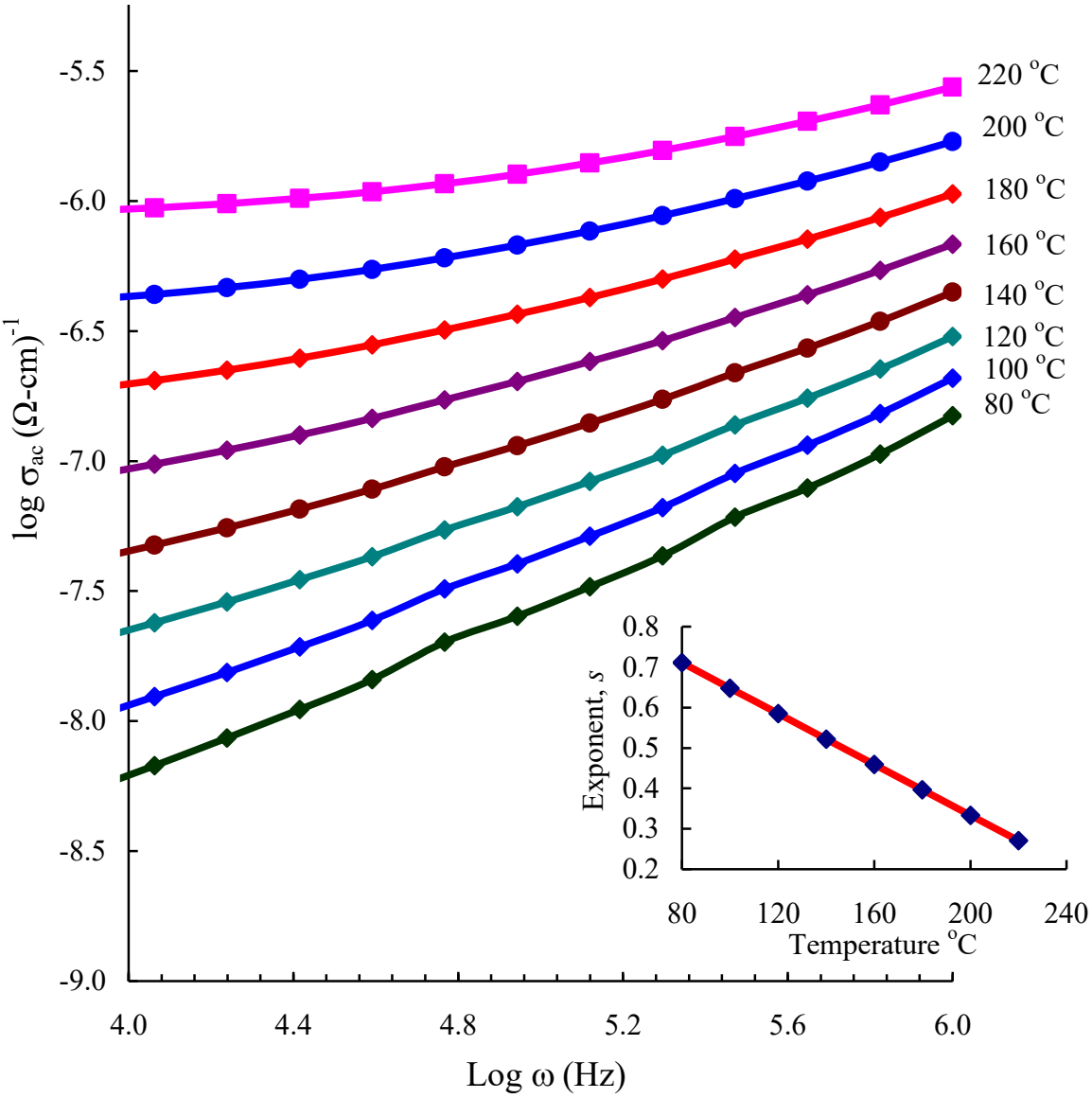

Fig. 17 Plots of log σ_{ac} (ω) versus log ω for the glass sample Au_6 drawn at different temperatures to evaluate frequency exponent *s*. Inset represents the variation of *s* with the temperature.